

HYDRODYNAMIC MODELS OF RADIO GALAXY MORPHOLOGY: WINGED AND X-SHAPED SOURCES

EDMUND J. HODGES-KLUCK¹ & CHRISTOPHER S. REYNOLDS¹

Department of Astronomy, University of Maryland, College Park, MD 20742-2421, USA

Accepted by ApJ 3/22/11

ABSTRACT

We present three-dimensional hydrodynamic models of radio galaxies interacting with initially relaxed hot atmospheres and explore the significant off-axis radio lobe structures which result under certain conditions. With a focus on the “winged” and “X-shaped” radio galaxy population, we confirm the importance of observed trends such as the connection of wing formation with jets co-aligned with the major axis of the surrounding atmosphere. These wings are formed substantially by the deflection of lobe plasma flowing back from the hot spots (backflow) and develop in two stages: supersonic expansion of an overpressured cocoon at early times followed by buoyant expansion at later times. We explore a limited parameter space of jet and atmosphere properties and find that the most prominent wings are produced when a decaying jet is injected into a small, dense, highly elliptical atmosphere. On the basis of this search, we argue that the deflection of backflow by gradients in the hot atmosphere is a strong candidate for forming observed wings but must work in tandem with some other mechanism for forming the initial wing channels. Our models indicate that lobe interaction with the hot atmosphere may play a dominant role in shaping the morphology of radio galaxies.

Subject headings: galaxies: jets – galaxies: active – hydrodynamics – galaxies: clusters: intracluster medium

1. INTRODUCTION

Recently, X-shaped radio galaxies (XRGs)—a peculiar class of radio galaxies with two pairs of misaligned lobes (Ekers et al. 1978; Leahy & Parma 1992)—have received significant attention as new observations have explored and critiqued the competing models for the origin of their odd morphology. The distinctive “X” shape occurs due to the intersection of two centro-symmetric synchrotron-emitting structures at a common nucleus (e.g. Figure 1). One of these structures is associated with an active relativistic jet (the “primary” lobes) whereas the other is fainter, more ragged, and does not appear to harbor a jet (the “secondary” lobes or “wings”). The wings can be long, collimated, and symmetric about the nucleus, and may even exhibit Z-shaped morphology of their own (Gopal-Krishna et al. 2003). The origin of the wings is not presently understood, but XRGs share other characteristics which indicate a common origin.

X-shaped sources make up about 5–10% of Fanaroff-Riley Type II (FR II; Fanaroff & Riley 1974) radio galaxies (e.g. Leahy & Parma 1992). The consensus sample is fairly small, but with the identification of ~ 100 “candidate” XRGs (Cheung 2007), a search for trends is now possible. Based on the combined consensus and candidate sample, XRGs tend to have radio powers and host optical luminosities near the FR I/II “break” in a Ledlow-Owen radio power–visual magnitude (Ledlow & Owen 1996) type plot (Cheung et al. 2009; Landt et al. 2010), and reside in elliptical galaxies with larger-than-average black hole masses (inferred from the $M - \sigma$ relation and broad lines from the active galactic nucleus; Mezcuca et al. 2010). XRGs do not seem to be in galaxies currently undergoing a merger based on inferred starburst history (Mezcuca et al. 2010) and a spectroscopic search for broad emission lines and

dusty nuclei (Landt et al. 2010), but the dynamic ages of their active lobes are younger than the age of the starburst (Mezcuca et al. 2010). The wings are preferentially co-aligned with the *minor* axis of the host, whereas the primary lobes tend to be co-aligned with the major axis (Capetti et al. 2002; Saripalli & Subrahmanyan 2009); this alignment has been confirmed in the X-rays which trace the distribution of hot gas in and around the host galaxies that provides the working surface which shapes the radio galaxy (Hodges-Kluck et al. 2010). The radiative age of the wings does not seem to follow a clear trend, as some wings have steeper spectral indices than the primary lobes (implying ageing) whereas others do not (Lal & Rao 2005). Notably, some wings are actually longer than the primary lobes, and wings are only found in radio galaxies with strong bridges.

A critical review of the observational data and existing models is found in Gopal-Krishna et al. (2010); here we briefly summarize the main threads. The origin of the secondary lobes has been attributed to (i) a rapid reorientation of the spin axis of the supermassive black hole (SMBH) powering the jet (i.e. the wings are fossils), either due to a SMBH merger (e.g. Rottmann 2001; Zier & Biermann 2001; Merritt & Ekers 2002) or rapid precession (e.g. Dennett-Thorpe et al. 2002); (ii) redirection and collimation of “backflow” (spent jet plasma flowing back from the terminal shocks) (Leahy & Williams 1984; Worrall et al. 1995; Capetti et al. 2002; Kraft et al. 2005); (iii) a binary AGN (Lal & Rao 2007); and (iv) interaction of the jet with disturbed morphology (e.g. stellar shells, phase-wrapped remnants of a merged disk galaxy; Gopal-Krishna et al. 2010). Since XRGs are usually strongly bridged sources and are apparently aware of their environments, it is worth examining closely the hypothesis that the X-shaped morphology originates from an interaction between the radio galaxy and its environment. In this pa-

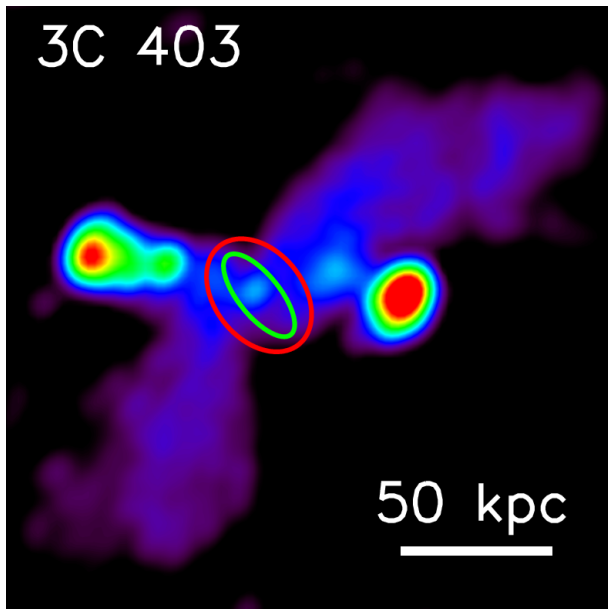


Figure 1. 3C 403, a typical XRG showing long, faint wings emanating from the same core as the edge-brightened lobes (east–west axis). The red and green ellipses have the ellipticity and position angle of the host galaxy and ISM (from Kraft et al. 2005) respectively (not to scale).

per, we seek to test the viability of the *backflow model* with three-dimensional hydrodynamic simulations in elliptical atmospheres.

In the backflow model, wings are produced by a single AGN outburst with powerful jets as the backflow is diverted along the steepest pressure gradient of the surrounding atmosphere (i.e. the minor axis). The wings either rise buoyantly or are driven in this direction (Leahy & Williams 1984; Worrall et al. 1995; Kraft et al. 2005) or form as supersonic outflows along the direction of least resistance from a ruptured over-pressured cocoon (Capetti et al. 2002; Zanni et al. 2003). These scenarios naturally explain the observed correlation between the wings and the minor axis as well as the dearth of strictly FR I XRGs (the weaker FR I sources do not produce powerful back-flows). However, the backflow model faces significant challenges, most notably the very long wings in many XRGs (often longer than the primary lobes). Whereas powerful jets are expected to drive through the surrounding medium supersonically, wings which expand buoyantly would do so at most transonically for most of their lives (Leahy & Parma 1992).

Because, in this model, fluid effects are primarily responsible for the “X” shape, hydrodynamic simulations are an ideal proving ground. Although recent hydrodynamic simulations of radio galaxy morphology exist in the literature, (e.g. Sutherland & Bicknell 2007; Falceta-Gonçalves et al. 2010; Gaibler et al. 2010), most are not concerned with the formation of lateral asymmetries such as wings. In view of advances in simulating radio galaxies in the past decade, the mounting evidence that XRGs constitute a population demands a critical look at the backflow model with new simulations. In

this paper, we discuss 3D hydrodynamic models of radio galaxies ignited in initially relaxed, elliptical atmospheres and examine how wings form.

We begin by discussing our simulation setup and strategy for exploring wing production in Section 2, then present our model runs and describe the evolution of a generic winged source in Section 3. In particular, we find that favorable pressure gradients are necessary but not sufficient to produce an X-shaped source; the character and time evolution of the jet is equally important. In Section 4, we briefly discuss the missing and artificial physics in our simulations, and in Section 5 we assess the backflow model in view of our results as well as discuss the implications for the broader picture of radio lobe morphology. Finally, in Section 6 we summarize our main results and conclusions.

Throughout this paper we use the terms “secondary lobes” and “wings” interchangeably. We also use the term “winged” source to refer to any radio source with substantial symmetric off-axis distortions whereas “X-shaped” sources are a subset of winged sources with an axial wing-to-lobe length ratio of more than 0.8. This nomenclature reflects the view of the hydrodynamic model in which XRGs are indeed a subset of a broader category of distortions. Finally, we use the term “backflows” to refer specifically to actual fluid flows heading back to the nucleus from the jet heads, whereas we use “backflow” to refer to the material in these flows.

2. HYDRODYNAMIC SIMULATIONS

We use a parallelized version of the ZEUS code (Stone & Norman 1992a,b) for our hydrodynamic simulations. ZEUS is a second-order (spatial accuracy) Eulerian finite-differencing magnetohydrodynamic (MHD) code which solves the standard equations of hydrodynamics,

$$\frac{\partial \rho}{\partial t} + \nabla \cdot (\rho \mathbf{v}) = 0 \quad (1)$$

$$\frac{\partial \mathbf{v}}{\partial t} + \mathbf{v} \cdot \nabla \mathbf{v} = -\frac{\nabla P}{\rho} - \nabla \Phi \quad (2)$$

$$\frac{\partial}{\partial t}(\rho e) + \nabla \cdot (\rho \mathbf{v} e) = -P \nabla \cdot \mathbf{v}, \quad (3)$$

for an ideal compressible fluid and introduces artificial viscosity for shocks. The version we use, ZEUS-MPv2, is based on the National Center for Supercomputing Applications (NCSA) code described in Hayes et al. (2006). We use spherical polar coordinates (r, θ, ϕ) in the purely hydrodynamical mode for all our runs; the jets are therefore injected from an inner boundary sphere with some small, but finite, radius r_{inner} . We outline our basic simulation setup below, followed by our strategy for exploring winged sources and a description of the evolution of a standard double-lobed source for comparison.

2.1. Simulation Setup

Hydrodynamic and MHD simulations of radio galaxies interacting with their surroundings are common due to the possibility that energy deposited by the lobes is a mode of heating in AGN feedback scenarios. We do not incorporate relativistic jet physics since we are primarily concerned with lobe mixing and evolution, but

the robustness of this assumption is explored in Section 4.1. We note here that non-relativistic, light, hypersonic hydrodynamic jets reproduce several essential features of jets. These include recollimation shocks, terminal shocks at the jet head (associated with radio “hot spots”) and back-flows of spent material from the terminal shocks which sheath the jet and produce lobes. Since we are interested in the evolution of back-flowing fluid in anisotropic environments, we adopt a non-relativistic purely hydrodynamic scheme.

We inject the jets as bi-directional flows into an initially hydrostatic, ellipsoidal atmosphere. The atmospheres we set up are ellipsoids with a polytropic equation of state ($\gamma = 5/3$) and a 3D β -model density profile (Cavaliere & Fusco-Femiano 1976) given by

$$\rho = \frac{\rho_0}{(1 + (r/r_0)^2)^{3\beta/2}}, \quad (4)$$

where $\beta = 0.5$, r_0 is the core radius, and ρ_0 is the core density. To adapt this model for elliptical atmospheres, we make the radial density profile dependent on angle by adding a major-axis position angle PA and ellipticity ϵ to the atmosphere, which we denote as r_e for an elliptical atmosphere. To easily allow for triaxial atmospheres, we define the ellipsoid in Cartesian space (x_e, y_e, z_e) and break up ϵ along each axis, then transform back to spherical coordinates to obtain the radius r_e using the grid coordinates (r, θ, ϕ):

$$r_e = \frac{\sqrt{x_e^2(1 - \epsilon_x)^2 + y_e^2(1 - \epsilon_y)^2 + z_e^2(1 - \epsilon_z)^2}}{(1 - \epsilon_{\max})} \quad (5)$$

$$x_e = r \sin(\theta) \left[\cos(\phi) \cos(\text{PA}) + \sin(\phi) \sin(\text{PA}) \right] \quad (6)$$

$$y_e = r \sin(\theta) \left[\sin(\phi) \cos(\text{PA}) - \cos(\phi) \sin(\text{PA}) \right] \quad (7)$$

$$z_e = r \cos(\theta) \left[\cos(\text{PA}) + \sin(\text{PA}) \right], \quad (8)$$

where PA is nominally measured clockwise from the z -axis (in practice, it is only the difference between the jet axis and the major axis of the ellipsoid that matters). To normalize the size of the atmosphere, ϵ_{\max} in Equation 5 is defined as the largest value of ϵ along each axis. For example, an atmosphere with large ϵ_z is elongated along the z -axis. Equations 4 and 5 may be understood as saying that introducing ϵ changes the effective core radius along a given axis: $r_{0,\text{eff}} = r_0(1 - \epsilon_{\max})/(1 - \epsilon)$. For example, if $\epsilon_{\max} = \epsilon_z = 0.75$, $\epsilon_x = 0.0$, and $r_0 = 1.0$, then along the z -axis $r_{0,\text{eff}} = 1.0$ and along the x -axis $r_{0,\text{eff}} = 0.25$. This phrasing is convenient when comparing the major and minor axes rather than the quantities along the full range of angles θ and ϕ and we use it hereafter.

The atmospheres are initially set up in hydrostatic equilibrium,

$$\nabla \Phi = \frac{1}{\rho} \nabla p, \quad (9)$$

assuming that the background dark matter potential is static and dominant so that the gas self-gravity is not important. We define the adiabatic sound speed $c_s \equiv 1.0$ in code units and set up an isothermal atmosphere so the

potential Φ is

$$\Phi = \frac{c_s^2}{\gamma} \ln(\rho) \quad (10)$$

Since XRGs are powerful radio galaxies and exist at low redshift, we assume a smooth intergalactic/intracluster medium (IGM/ICM) and gas-poor systems, i.e. no disk of colder (i.e. atomic or molecular) material in the host (c.f. Sutherland & Bicknell 2007). We note that in several exploratory runs, additional atmospheric complexity is overlaid onto a smooth atmosphere with no change in the gravitational potential Φ , i.e. not initially in hydrostatic equilibrium.

The jets in our simulations are hypersonic ($\sim 100c_s$) light ($\rho_{\text{jet}} \sim 0.01\rho_0$) flows injected in pressure equilibrium with the ambient material from back-to-back circular footpoints on the small inner boundary sphere at the origin. The kinetic luminosity of the jets is given by

$$L_{\text{kin}} \sim \frac{1}{2} \rho_{\text{jet}} v_{\text{jet}}^3 A_{\text{jet}} \quad (11)$$

where A_{jet} is the area of the footpoint at r_{inner} , and ignoring higher order contributions from the gravitational energy or thermal flux. To tune L_{kin} we primarily vary v_{jet} because (i) L_{kin} is most sensitive to changes in v_{jet} , (ii) the jets must be “light” to ensure that the Kelvin-Helmholtz instability growth rate at the boundary of the cocoon is approximately the same as in the relativistic case (Reynolds et al. 2002), and (iii) jets are highly collimated. The maximum jet width is constrained by high-resolution X-ray observations of jet knots (e.g. Perlman & Wilson 2005) and very long baseline interferometry observations of transverse structures (e.g. Gabuzda et al. 2004). However, we note that in Section 3.2 we vary ρ_{jet} and A_{jet} in a limited range.

We insist that the jet cover enough grid zones (~ 30) to resolve transverse structures such as the oblique shocks which collimate the jet. The jet is rapidly precessed around a small angle ($\alpha < \theta_{\text{jet}}$) at $20\pi \text{ rad s}^{-1}$ (code time) to break the axisymmetry of the simulation setup and simulate helical instabilities, thus spreading the thrust out over a larger working surface (c.f. Vernaleo & Reynolds 2006; Heinz et al. 2006; Sutherland & Bicknell 2007; O’Neill & Jones 2010). The location of the jet on the inflow sphere is thus given by $(\theta, \phi) = (\alpha, \Omega_{\text{jet}} \cdot t)$. Although the angular quantities are free parameters, they are constrained by the observed collimation of jets. Typical values are $\theta_{\text{jet}} = \pi/7.5$ and $\alpha = \pi/60$ for $r_{\text{inner}} = 0.05$. In agreement with other work, these jets develop a cylindrical core of fast-moving material sheathed in a slower concentric shell continuous at the boundaries with the surrounding material and core.

We use a grid with zones spaced according to a geometric series in r and θ (256 bins each) and uniformly in ϕ (64 bins). This grid resolves the internal jet structure and important processes near the injection footpoints. We choose $r \in [0.05, 5.0]$ and $\theta \in [0.01, 3.13]$ to avoid the polar singularity and begin with reasonably sized grid zones. The θ grid is broken into two symmetric 128-bin components with the smallest zones near the poles where the jets are injected. The adequacy of our grid is demonstrated by a run with double the resolution in each direction which produces similar internal jet struc-

ture. Mixing is not substantially different at the lobe boundaries.

We use periodic boundary conditions in the ϕ direction and reflecting boundary conditions in θ . The outer r boundary at $r = 5.0$ has outflow conditions (material leaving the grid); likewise, outflow conditions exist for all r_{inner} zones except where the jets are injected. The outer boundary is far from the jet activity so negligible material leaves the grid there. We discuss the importance of the inner boundary sphere in Section 4.

Code units are transformed to physical units by choosing appropriate values for r_0 , c_s , and ρ_0 . For instance, Reynolds et al. (2002) defined $r_0 = 100$ kpc, $c_s = 1000$ km s $^{-1}$ and $\rho_0 = 0.01 m_{\text{H}}$ g cm $^{-3}$ for a rich cluster and $r_0 = 10$ kpc, $c_s = 500$ km s $^{-1}$ and $\rho_0 = 0.1 m_{\text{H}}$ g cm $^{-3}$ for a group or poor cluster. In the former scheme a code unit of time (derived from the crossing time) corresponds to 50 Myr and in the latter 10 Myr. In our runs, we vary r_0 and ρ_0 but fix c_s ; a value of $c_s \sim 500$ km s $^{-1}$ appears appropriate for XRGs based on temperatures derived from spectral fitting (Hodges-Kluck et al. 2010; Landt et al. 2010). A jet injected at $100c_s$ would then have a physical speed between $0.17c - 0.35c$ (a Lorentz factor of $\gamma \sim 1.01 - 1.05$). However, as noted by Komissarov & Falle (1996), comparing classical and relativistic jet simulations requires careful matching of parameters, in particular the mass-energy density content of the jet. Hence, the jet velocities chosen should not be taken directly as assumptions of true jet velocity.

Our runs were parallelized and used variety of processors. Many of the runs were conducted on quad-core Intel[®] Core[™] 2.4 and 2.83 GHz workstations.

2.2. Strategy

We now outline our guiding strategy to determine whether X-shaped sources can result from the interaction of radio galaxy lobes with their environment.

First, we only model powerful FR II sources which produce strong back-flows. Neither the physical origin of the FR I/II dichotomy nor the differences between jets in radio loud and radio quiet sources are understood, but the higher luminosity FR IIs exhibit the hot spots, well defined lobes, and bridges exploited by the backflow model.

In accordance with the observations (Capetti et al. 2002; Saripalli & Subrahmanyan 2009; Hodges-Kluck et al. 2010), we inject jets along the major axis of the surrounding atmosphere. We first use unrealistic atmospheres with very favorable pressure gradients for wing production (as in Capetti et al. 2002), then explore jet and atmosphere parameters to study the production and characteristics of XRGs. In particular, we explore the dependence of wing formation on jet width, density, and kinetic luminosity as a function of time, and initial atmosphere parameters (core radius, density, ellipticity, and position angle). Although some parameter combinations are degenerate, this is a very large parameter space because the $L_{\text{kin}}(t)$ may include dead time and intermittency. Compared to 2D modeling, our 3D simulations eliminate the requirement of axisymmetry which enhances the jet head advance speed (Bodo et al. 1998) and the coherence of the back-flows. The effect of turbulence is also more

realistically explored in three dimensions.

Motivated by the expectation that pressure gradients affect the wings fundamentally the same way in different systems, we start from the ansatz that jet and atmospheric parameters are orthogonal. In other words, the jet parameters may be tuned in some fiducial atmosphere and the atmosphere parameters may be tuned with some fiducial jet such that the behavior of an arbitrary jet in an arbitrary atmosphere can be inferred. On the basis of this method we will evaluate the factors key to wing prominence and the viability of the backflow models.

2.3. Hydrodynamic Models of Powerful Double-Lobed Radio Galaxies

If wings are distortions to a generic double-lobed source, we expect our simulated radio galaxies to strongly resemble the double-lobed sources produced by earlier models. Hydrodynamic and MHD models of jets are commonly employed to study either the phenomenology of the jets and lobes (with relativistic and nonrelativistic fluids) or the energy deposited by the lobes into their environment. Hence, a large body of work concerned with phenomenological models of these sources exists and has produced key insights into the life of a powerful radio source.

These studies include work on early jet/lobe evolution in a relaxed atmosphere (e.g. Krause 2005; Antonuccio-Delogu & Silk 2010), the influence of the ρ_{jet}/ρ_0 density contrast and internal Mach number (e.g. Carvalho & O’Dea 2002a; Krause 2003; Vernaleo & Reynolds 2007), jet stability in nonrelativistic and relativistic conditions (e.g. Rosen et al. 1999; Keppens et al. 2008; O’Neill & Jones 2010; Mignone et al. 2010), the importance of intermittency (O’Neill & Jones 2010) or intrinsically spreading out the jet thrust to slow the advance of simulated jets (e.g. Heinz et al. 2006), the importance of the jet environment to morphology or energy deposition (e.g. Capetti et al. 2002; Carvalho & O’Dea 2002b; Krause 2005; Zier 2005; Vernaleo & Reynolds 2007; Simionescu et al. 2009; Kawakatu et al. 2009; Falceta-Gonçalves et al. 2010; Gaibler et al. 2010), and physics beyond MHD (e.g. Saxton et al. 2010). Naturally, there is overlap between the phenomenological studies and those motivated by the challenge to produce jets which prevent a cooling catastrophe in the ICM of a host galaxy cluster by isotropizing energy distribution. The viability of radio galaxies as AGN feedback mechanisms is beyond the scope of this work, but jet lifetime and the passive evolution of “dead” radio galaxies (Reynolds et al. 2002) place important constraints on wing prominence.

Based on this work, we understand a powerful double-lobed source to have three distinct phases of evolution: (i) *ignition*, in which a spheroidal cocoon of relativistic plasma is formed around the nascent jets, (ii) the *active phase*, wherein the jet produces the cigar-shaped lobes associated with FR II radio galaxies, and (iii) the *passive phase* where lobes evolve after the jet is turned off. Below we outline these phases for a preliminary hydrodynamical simulation of a fast ($v_{\text{jet}} = 100c_s \exp(-3t)$), light jet with large L_{kin} (a “FR II” source) to provide a framework for discussing the evolution of winged sources (left-

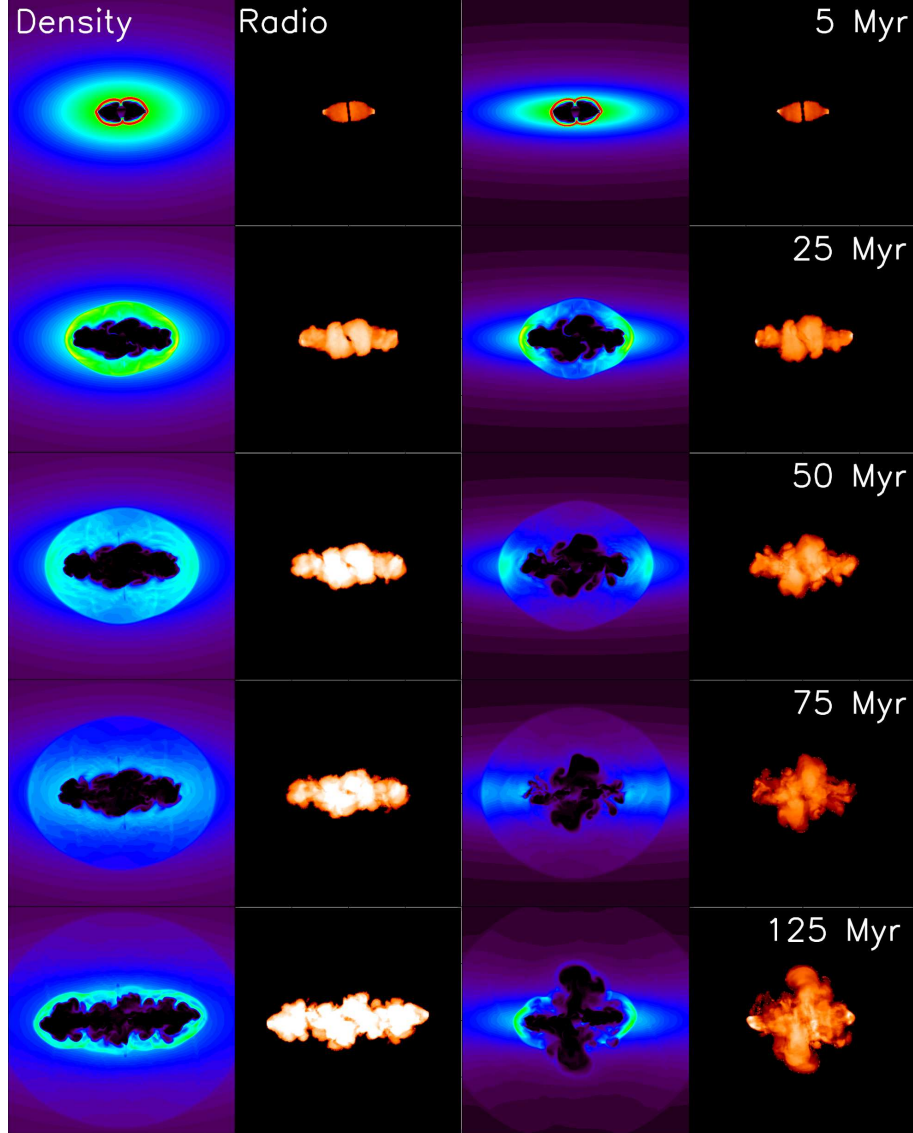


Figure 2. Comparison of a normal (left panels) and winged (right panels) radio source using the same jet ($v_{\text{jet}} = 100 \exp[-3t]$) in atmospheres differentiated only by ϵ . Note the size of the overpressured cocoon relative to the size of the atmosphere in the top panels. At a code time of 1.0 (100 Myr) the jet was restarted ($v_{\text{jet}} = 100 \exp[-3(t - 1.0)]$). The colorbars are the same in each image; the integrated radio is brighter for the normal source because the winged source has the same amount of material spread out over more volume.

hand panels of Figure 2.2). We note that Belan et al. (2011) have recently found good agreement between the structures observed in hydrodynamic simulations of hypersonic jets and laboratory experiment.

Ignition— The jet is injected in pressure equilibrium with the initially relaxed surrounding medium. The flow quickly forms and drives a spheroidal bow shock into the surrounding medium (Figure 2.2, top left panel). At the location where the jet impacts the shock, back-flows develop which fill the space evacuated by the bow shock with light, hot spent jet plasma. This plasma forms a cocoon which sheaths the jet. At very early times the jet expands laterally, since it is unconfined by the cocoon plasma (in part due to the initially conical shape of the jet) and the expansion of the nascent radio galaxy is nearly self-similar (Carvalho & O’Dea 2002a; Krause 2005). However, as a result, the early back-flows

acquire a circulatory motion and flow along the inner edge of the bow shock (Figure 3, top panel). By the time these flows reach the midplane between the two jets, they have velocity vectors pointing radially inwards and do not collide with back-flows from the counter-jet (Antonuccio-Delogu & Silk 2010). In our models, the back-flows are also prevented from interacting with their counterparts from the counter-jet because our jets are injected into pristine atmospheres such that at very early times, each jet inflates its own cocoon. The two cocoons are both bounded by a bow shock, and the two shocks meet at the midplane between the jets and form an interstice of dense material that prevents early mixing (Figure 3, top panel). Whether such an interstice is present in real sources is not clear (we do not resolve the very earliest jet stages such as the “flood-and-channel” phase seen in a clumpy, warm disk in Sutherland & Bicknell 2007), but the interstice is ablated and the cocoon is

unified by the active phase.

As the cocoon pressure builds due to backflow confined by the bow shocks, the jet becomes azimuthally confined and a recollimation shock appears near the injection point; by the end of the ignition phase, the cocoon is strongly overpressured relative to its environment. At the same time, the terminal shock becomes increasingly distinct from the bow shock, and the jet head takes on the characteristic double-pronged appearance of a 3D hydrodynamical jet. While the back-flows still follow the bow shocks during the late ignition phase, they are increasingly straight. We note that this early evolution is seen in all our runs and does not depend much on atmosphere or jet parameters, nor on the boundary conditions (as long as the core radius of the atmosphere r_0 is much larger than r_{inner}).

Active Phase— When the jet head overtakes and pierces the initial bow shocks (driving a bow shock contiguous with the initial burst; Krause 2005), the active phase begins and a classical radio galaxy develops, with a cigar-shaped cocoon, hot spots, bow shocks (middle-left panels of Figure 2.2), and straight back-flows (Figure 3, bottom panel). At this point, the cocoon ceases to be substantially overpressured and the cocoon’s lateral expansion falls close to the sound speed of the ambient medium, lagging behind the bow shock (the cocoon expands due to buoyancy, Kelvin-Helmholtz, and Rayleigh-Taylor instabilities). This weak shock ($v_{\text{shock}} \sim 1.5c_s$) sweeps up a large amount of material as it expands and becomes better described as a strong sound wave (Figure 2.2). Meanwhile, the jet develops internal oblique collimating shocks along its length, retaining a high velocity out to the terminal shock at the jet head (i.e. the angular size of the jet decreases with increasing radius) where the cocoon becomes momentum-driven. Less powerful jets do not produce cocoons (Vernaleo & Reynolds 2007), but we focus on the cocoon-bounded case (the cocoon pressure also depends on the internal Mach number; Carvalho & O’Dea 2002a).

Passive Phase— Once the jets are turned off, the back-flows cease and the “dead” radio galaxy rises buoyantly in the atmosphere, lifting large amounts of material to great heights and mixing with the surrounding medium (Reynolds et al. 2002). Although the radio galaxy is relatively efficient at depositing its energy irreversibly in the surrounding medium, it is difficult to isotropize this energy deposition on short enough timescales to avoid a cooling catastrophes (e.g. Reynolds et al. 2002; Omma et al. 2004; Omma & Binney 2004; Vernaleo & Reynolds 2006, 2007; O’Neill et al. 2005; De Young 2010; O’Neill & Jones 2010; Ostriker et al. 2010). The cocoon separates into bubbles which pinch off along the direction of the jets and rise in opposite directions; the evolution of these bubbles may be quite complex (e.g. Begelman 2001; Churazov et al. 2001; Ruszkowski et al. 2007; Dong & Stone 2009; O’Neill et al. 2009; Braithwaite 2010; Pope et al. 2010). This very late stage evolution is unlikely to be important for winged galaxy evolution, as winged galaxies appear to be related to sources with strong bridges (Leahy & Williams 1984), and is not shown in Figure 2.2.

3. RESULTS

With the scheme described in Section 2, we produce winged radio galaxies by the deflection of backflow into channels perpendicular to the jets. In our models, wings are produced in strongly asymmetric atmospheres when the jet is driven near the major axis; the wings are produced along the minor axis as cocoon material escapes the central regions of the atmosphere and evolve buoyantly, collimated by the surrounding stratified atmosphere which promotes expansion along the steepest pressure gradient. Hence, these wings are similar to those produced by Capetti et al. (2002) and Zanni et al. (2003). Without introducing additional complexity to the atmosphere, hydrodynamic wings are formed in two stages. First, during the ignition phase (Section 2.3), the overpressured cocoon expands faster along the minor axis due to the steeper pressure gradient and forms small channels (proto-wings) perpendicular to the jet into which back-flowing plasma flows. The proto-wings produced in this way can account for 20–40% of wing length at the end of the active phase depending on the gradient. Second, during the active phase, the wings rise buoyantly, fed by turbulent flows near the midplane. Although the back-flows near the jet heads are initially laminar and supersonic (relative to the lobe material), they quickly decelerate and do not enter the wings as coherent flows; the wings expand subsonically.

During the active phase the wings evolve almost independently of the cocoon. Hence, once wings have developed, their length depends only on the properties of the native atmosphere whereas the length of the jet-fed primary lobes is dominated by the properties of the jet (in particular the kinetic luminosity as a function of time) for powerful jets. Therefore, *decaying* jets produce prominent wings.

In this section, we explore these ideas in detail, first comparing the life of a winged source to a canonical double-lobed one (Figure 2.2) and then looking at the dependence of wing prominence and longevity on various tunable parameters in our models.

3.1. Evolution of a Winged Source

Winged galaxies experience the same life stages outlined in Section 2.3. We describe how wings fit into this process in detail below, referencing our standard (extremal) atmosphere (Run STANDARD, Tables 1 and 2). While unrealistic, this atmosphere provides important insights into the backflow model and can be directly compared to prior work (Capetti et al. 2002; Zanni et al. 2003).

Ignition— During the ignition phase of a winged source, the anisotropic expansion of the overpressured cocoon in an aspherical atmosphere produces channels which will later become the wings (the proto-wings). This pressure-driven expansion is supersonic but brief, since the cocoon quickly reaches pressure equilibrium. Although these channels need not be produced by an overpressured cocoon, some channels must exist for wings to form.

The degree of cocoon expansion in a given direction depends on the pressure gradient experienced in that direction, and hence on the atmospheric parameters. In particular, the eccentricity of the atmosphere effectively changes the core radius r_0 seen by the cocoon in different

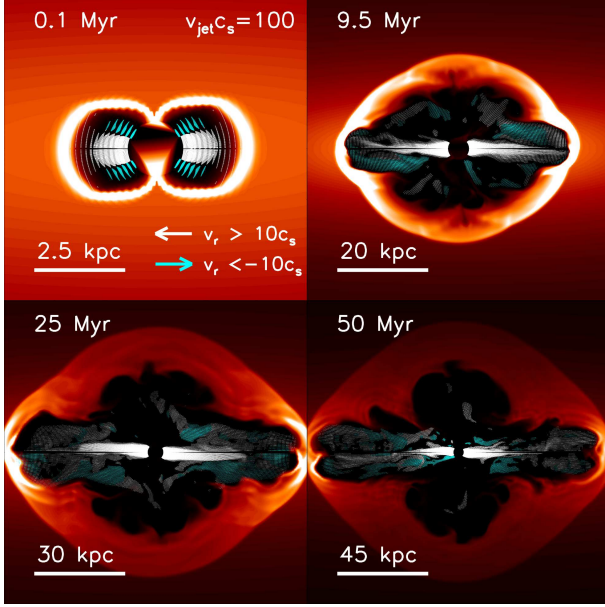


Figure 3. We show here v_x and v_y velocity vectors overlaid on density slices (taken at $\phi = 0$) at different times for the simulation TX_E75_VE3_B5.0 (Table 3). We have chosen (arbitrarily) $c_s = 500 \text{ km s}^{-1}$ and $r_0 = 50 \text{ kpc}$ (corresponding to a code $r_0 = 2.0$) to represent a large elliptical galaxy. White vectors point radially outwards and cyan vectors point radially inwards (i.e. the back-flows). Vectors are only shown when the magnitude of v exceeds the sound speed of the lobe material ($c_{s,\text{lobe}} = 10c_s$). Note that early on, the back-flows follow the contact discontinuity and are directed towards the inner boundary, but later become straight as in Antonuccio-Delogu & Silk (2010).

directions. For example, along the x -axis ($r\hat{x}$; the jet is driven along \hat{z}) Equation 4 gives:

$$\frac{\partial p}{\partial x} = -\frac{3}{2} \frac{c_s^2}{\gamma} \rho_0^{3/2} \frac{x}{r_{0,\text{eff}}^2 (x^2 + r_{0,\text{eff}}^2)^{7/4}}. \quad (12)$$

where $r_{0,\text{eff}} = r_0(1 - \epsilon_{\text{max}})/(1 - \epsilon_x)$ as above. Since the pressure gradient is steeper for smaller $r_{0,\text{eff}}$, higher ellipticity along other axes promotes wing expansion: for $\epsilon_x = 0.0$ and $\epsilon_z = \epsilon_{\text{max}} = 0.75$, $r_{0,\text{eff}} = 0.25r_0$ along the x -axis. Conversely, if $\epsilon_x = \epsilon_{\text{max}} = 0.75$ and $\epsilon_z = 0.0$ (the jet is pointed along the minor axis), $r_{0,\text{eff}} = r_0$ and wings are suppressed. Of course, wing expansion depends on the actual pressure gradients rather than just the ratio along different axes; the base values r_0 and ρ_0 determine whether wings can form (i.e. a highly elliptical atmosphere can have shallow pressure gradients along the minor axis if it is very large). Note that at very small radii $r \ll r_{0,\text{eff}}$ (i.e. during the ignition phase), the pressure gradient steepens linearly with increasing r and at large radii (during the active phase, see below) the pressure gradient becomes shallower as $r^{-1/2}$. Hence, the ignition phase is the time at which atmospheric asymmetry has the strongest effect on the ultimate morphology of the source.

Active Phase— Once the cocoon has reached pressure equilibrium, the proto-wings are no longer pressure-driven. As the back-flows become straight, they merge and fill the channels (Figure 3, bottom panel) to form

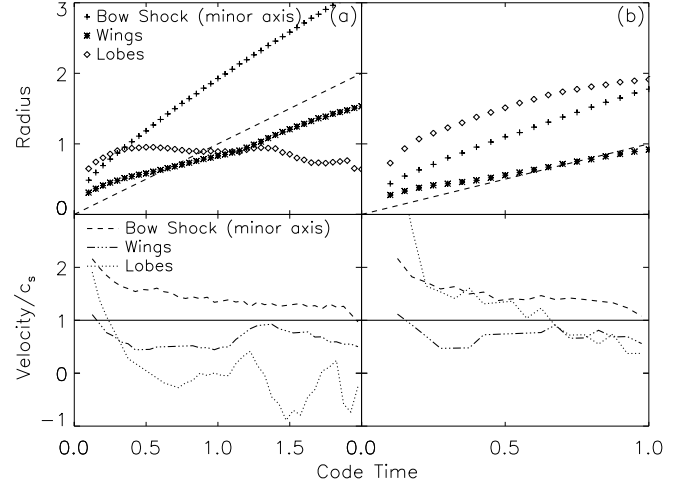


Figure 4. Positions and velocities of the leading edges of the bow shock, wings, and lobes shown for (a) the standard simulation and (b) a triaxial simulation. The dashed line in the top panel shows the position of a point moving radially outwards at the sound speed. Note the different x -axes; at $t = 1.0$ in the left panels, a new jet is reinjected. *Negative* growth for the lobes indicates collapse during the passive phase.

structures more closely resembling observed wings. However, the flows into the wings are turbulent and transonic or subsonic (relative to the internal lobe sound speed $c_{s,\text{lobe}} = 10c_s$). In other words, wings are not *driven* during the active phase. Rather, because they are structures filled with light fluid, they rise buoyantly in the atmosphere, collimated by the stratified elliptical atmosphere.

Since the wings rise buoyantly, their growth rate is subsonic. To see this, it is instructive to look at the simplified case of a spherical bubble (of fixed radius) rising buoyantly in a dense fluid. The (terminal) buoyant velocity at a given height for such a bubble is

$$v_{\text{buoy}} = \sqrt{\frac{2gV_b}{C_D A_b}} = c_s \sqrt{\frac{16}{3\gamma} \frac{r_b}{r_{0,\text{eff}}^2} \frac{r}{1 + (r/r_{0,\text{eff}})^2}} \quad (13)$$

where V_b , A_b , and r_b are the volume, cross-sectional area, and radius of the bubble respectively, $C_D = 0.75$ is the “drag” coefficient, and we have used the background dark matter potential Φ to compute g in terms of r and effective core radius $r_{0,\text{eff}} = r_0(1 - \epsilon_{\text{max}})/(1 - \epsilon)$. Naturally, this follows the pressure gradient (Equation 12), so when the bubble is at very small radii its velocity *increases* as $r^{1/2}$, whereas outside $r_{0,\text{eff}}$ it *decreases* as $r^{-1/2}$. For typical values in our simulations, the peak value of v_{buoy} is approximately c_s . Hence, in a highly elliptical atmosphere, a bubble rising along the minor axis will rise subsonically with decreasing velocity for most of its lifetime.

Our wings do not fit this simplified case because they are large relative to $r_{0,\text{eff}}$, variable in size, aspherical, and connected to the cocoon. Nonetheless, their expansion is subsonic for the same reason: the wings exceed $r_{0,\text{eff}}$ early on when their growth is pressure-driven rather than buoyant, and v_{buoy} monotonically declines thereafter. This transition from supersonic to subsonic wing expansion is plainly seen in Figure 4.

Therefore, wings in our models may not intrinsically exceed the length of the primary lobes unless the primary

lobes advance at some average speed $\bar{v}_h < c_s$. Since powerful jets are required to produce the proto-wings in an overpressured cocoon phase, prominent wings require decaying jets, intermittent jets, or jets which deposit their thrust over an increasingly large area with time. The profile of the fiducial run is shown along with its wing prominence in Figure 5 and compared to a triaxial atmosphere in Figure 4. Note that in the fiducial run (left panel of Figure 4) the wings eventually overtake the lobes (in part due to the collapse of the lobes when the jet is very weak), but clearly move into a subsonic regime early and remain there. The bow shock remains mildly supersonic through most of both simulations. In Figure 6 we show wings produced by decaying jets during the active phase in several environments (the fiducial run is shown in the top row).

Passive Phase— Once the jets are turned off, the cocoon disintegrates as the lobes either rise buoyantly as bubbles or collapse under the relaxing atmosphere. If the radio galaxy is within a few r_0 in a dense atmosphere, the fallback of displaced material shreds the lobes into small bubbles. In either case, the wings pinch off and rise. These bubbles do not survive long, but their behavior might be substantially altered in the presence of magnetic fields (e.g. O’Neill et al. 2005; Braithwaite 2010; Pope et al. 2010). Because observed winged sources have strong bridges, we expect them to be in the active phase.

Reinjection— A powerful jet reignited during the passive phase before the cocoon has disintegrated may significantly enhance the wings. If the old jet channel is somewhat broken up, the reinjected jet forms a new terminal shock and bow shocks *inside* the old cocoon. These new shocks do not form spheroidal structures (as in a relaxed atmosphere) but instead produce strong, straight back-flows near the midplane. Hence, the wings receive a large influx of fresh supersonic plasma directly after reinjection (Figure 2.2, bottom panels). This brightens the wings substantially and reinforces their structures.

There is a relatively narrow window of time where this process is effective. If the reinjection occurs while the jet channels are largely intact (i.e. during the active phase), the jet simply follows these channels. On the other hand, if the reinjection occurs when the wings have already separated from the lobes as individual bubbles, the new jet cannot feed them. Even if the reinjection occurs at the “right” time, the efficacy of the restarted jet at promoting wings is short-lived. However, this mechanism can produce wings that are intrinsically *longer* than the jet-driven lobes (Figure 3, bottom panels). If the reinjected jet decays, this extreme axial ratio can be maintained for most of the lifetime of the restarted radio galaxy and a bona-fide X-shaped source results, although this source would only have the “FR II” primary lobes for a short period of time (~ 5 Myr for a source 40 kpc across).

3.2. Ecology of Winged Sources

In Section 3.1, we describe the life stages of a winged radio source. We now describe the dependence of wing prominence on our tunable parameters. Following the strategy laid out in Section 2.2, we begin with the fiducial simulation **STANDARD** which is characterized by an atmosphere with a large ellipticity ϵ and a jet with a

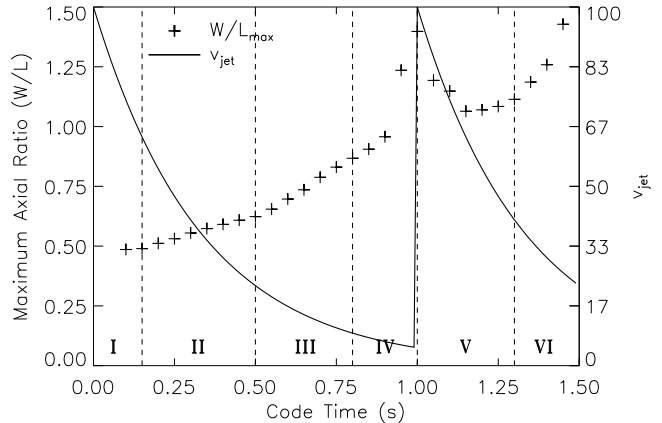


Figure 5. Plot of W/L_{\max} (crosses) in timestep intervals of $\delta t = 0.05$ for the standard simulation with a reinjection at $t = 1.0$. We have overplotted the velocity of the jet as the black line (right y -axis). The Roman numerals indicate (I) the overpressured cocoon phase, (II) the active phase (powerful jet), (III) the active phase (weak jet), (IV) the passive phase (with cocoon collapse), (V) a second active phase due to the reinjected jet, and (VI) the second passive phase with further cocoon collapse. During cocoon collapse, the source does not resemble a winged source (instead it is a “dead” radio galaxy). A source appears winged during the active phase when the jet is most like a weak FR II or strong FR I.

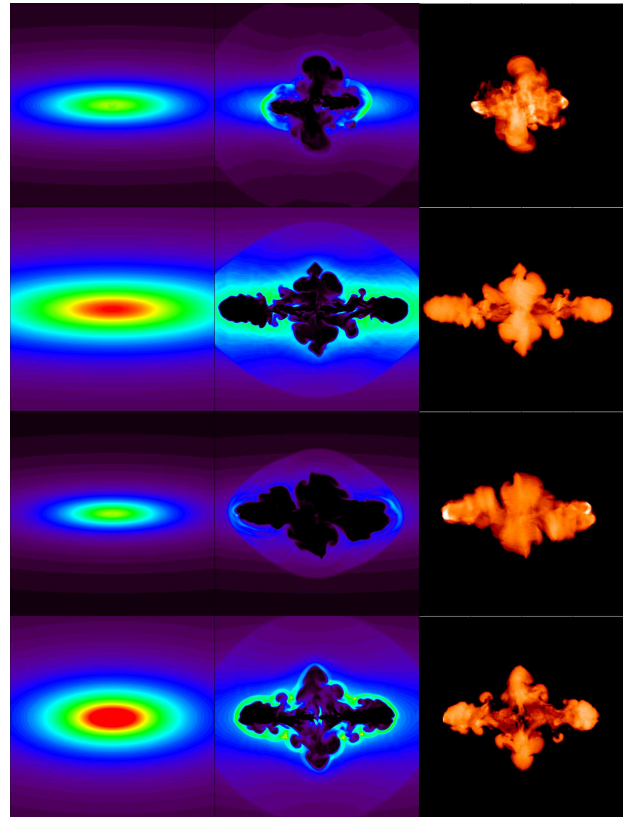


Figure 6. Examples of different intrinsic wing morphology. Left: Initial relaxed atmosphere density. Center: Winged sources during the late active phase. Right: False synchrotron maps ($j_\nu \propto p/\rho^{7/4}$ assuming equipartition) of these sources.

velocity profile $v_{\text{jet}} = 100c_s \exp[-3t]$ (Figures 2.2 and 4). Taking the jet from the fiducial run, we individually vary parameters in the atmosphere in order to see their influence on wings (Figure 7, Table 1), and then vary jet parameters in the fiducial atmosphere (Figure 8, Table 2). We then synthesize the information gleaned from these single-parameter curves to attempt to find atmospheres and jets which can explain real winged sources, including more complex behavior as well (Table 3). All of the runs proceed to a code time of 1.0 or more, where most have entered the passive phase. Reinjections, where used, occur near the beginning of the passive phase.

To quantify wing prominence we use the wing-to-lobe axial ratio (W/L). This quantity is an imperfect measure because W/L intrinsically varies with azimuthal angle ϕ and time, and observable sources are seen in projection so the observed W/L will differ from the intrinsic value. W/L is also essentially meaningless during ignition or the passive phase, but a source in one of these stages would not be classified as “winged.” For the parameter exploration in Figures 7 and 8 (values in Tables 1 and 2), we adopt as a fiducial value $W/L_{0.5}$: the maximum intrinsic W/L for any pair of azimuthal angles $[\phi, \phi + \pi]$ at a code time $t = 0.5$. For the standard jet ($v_{\text{jet}} = 100c_s \exp[-3t]$), $t = 0.5$ represents the transition from a powerful to weak jet in the active phase, and by this time the wings have begun to grow buoyantly. Hence, a code time of $t = 0.5$ is a reasonable place to measure the influence of the atmosphere on wings. We also use $W/L_{0.5}$ in varying the jet parameters, noting that while $t = 0.5$ is no longer special, all of the runs in Table 2 are in the active phase at this time. $W/L_{0.5}$ is not predictive of wing length later in the same simulation, but is a good measure of relative wing prominence between simulations due to the subsonic growth of wings.

From Figure 7 one can get a broad sense of the dependence of wing prominence on the size and shape of the atmosphere. It is immediately obvious that there is a strong dependence on the ellipticity ϵ of the atmosphere, and that smaller, denser atmospheres are the most conducive to wing formation (although “small” could be physically quite large depending on the jet). It is also notable that relatively high values of W/L can be achieved by $t = 0.5$; because we use a decaying jet, the wings will only become more prominent during the later active phase. While these results are not surprising (Equation 12), the particular form of the curves depends on both the jet and the atmosphere. As expected from Capetti et al. (2002) and Saripalli & Subrahmanyan (2009), long wings require jets co-aligned close to the major axis.

The trends are less clear when varying jet parameters (Figure 8). In the top panels, the jet velocity is allowed to vary freely without conserving integrated kinetic luminosity between runs. If the jet is injected at constant velocity throughout the simulation (Figure 8a), a faster jet is slightly better than a slower one at making wings. However, a decaying jet (Figure 8b) is better still, with pure exponential decay more effective at increasing $W/L_{0.5}$ than “Gaussian” jets of the form $v_{\text{jet}} = v_0 \exp[-at^2]$. In the bottom panels of Figure 8, we hold the kinetic luminosity constant between runs by modifying v_0 . From Figure 8c, it is evident that in-

Table 1
Varying the Atmosphere using the Standard Jet

Name	Wings?	r_0	ρ_0	ϵ_x	ϵ_z	ΔPA (deg.)	W/L ($t = 0.5$)
Standard Atmosphere							
STANDARD	Y	1.0	3.0	0.0	0.75	0.0	0.62
Ellipticity							
SJ_E20	N	1.0	3.0	0.0	0.20	0.0	0.42
SJ_E30	N	1.0	3.0	0.0	0.30	0.0	0.43
SJ_E50	N	1.0	3.0	0.0	0.50	0.0	0.49
SJ_E60	Y	1.0	3.0	0.0	0.60	0.0	0.54
Core Radius							
SJ_R0.5	Y	0.5	3.0	0.0	0.75	0.0	0.73
SJ_R0.75	Y	0.75	3.0	0.0	0.75	0.0	0.61
SJ_R2.0	N	2.0	3.0	0.0	0.75	0.0	0.45
Core Density							
SJ_D1.5	Y	1.0	1.5	0.0	0.75	0.0	0.52
SJ_D2.0	Y	1.0	2.0	0.0	0.75	0.0	0.57
SJ_D4.0	Y	1.0	4.0	0.0	0.75	0.0	0.65
SJ_D5.0	Y	1.0	5.0	0.0	0.75	0.0	0.68
ΔPA							
SJ_PA5	Y	1.0	3.0	0.0	0.75	5.0	0.62
SJ_PA10	Y	1.0	3.0	0.0	0.75	10.0	0.60
SJ_PA15	Y	1.0	3.0	0.0	0.75	15.0	0.58
SJ_PA20	Y	1.0	3.0	0.0	0.75	20.0	0.51
Triaxial Atmospheres							
TX_E75_1	Y	1.0	3.0	0.375	0.75	0.0	0.65
TX_E75_2	Y	1.0	3.0	0.50	0.75	0.0	0.72

Note. — Runs in which the standard atmosphere was varied one parameter at a time, holding the standard jet ($v_{\text{jet}} = 100c_s \exp[-3t]$, $\alpha = \pi/35$ rad and $\beta = \pi/15$ rad for $r_{\text{inner}} = 0.1$) constant. The STANDARD run uses the standard jet and atmosphere and hence is a data point in each category. The “wings” column denotes whether a run produced noticeable wings at any point during its active lifetime. W/L at $t = 0.5$, on the other hand, is a way to directly compare different runs. At $t = 0.5$, $v_{\text{jet}} \sim 20c_s$, i.e. twice the lobe material sound speed and a transition point during the active phase between a powerful and weak jet. The time of this transition depends on the velocity profile of the jet; $t = 0.5$ is only correct for the standard jet. ΔPA is the angular distance between the jet and the major axis.

creasing the width of the jet (at the cost of a slower jet) is important. Changing the density of the jet material has an extreme effect on $W/L_{0.5}$ (Figure 8d); above $\rho_{\text{jet}} \sim 0.01$, the jet ceases to be “light” relative to the background and no longer forms lobes resembling radio galaxies (Reynolds et al. 2002). At very low densities, mixing becomes very efficient at disrupting the radio galaxy.

We now discuss these results in detail, beginning with the properties of the fiducial run.

Fiducial Run— Our fiducial run (STANDARD, Tables 1 and 2) is the combination of our fiducial atmosphere ($r_0 = 1.0$, $\rho_0 = 3.0$, $\epsilon_x = \epsilon_y = 0.0$, $\epsilon_z = 0.75$) with our fiducial jet ($v_{\text{jet}} = 100c_s \exp[-3t]$, $\theta_{\text{jet}} = \pi/15$, $\alpha = \pi/35$, aligned along the z -axis). Like most of our runs, this simulation

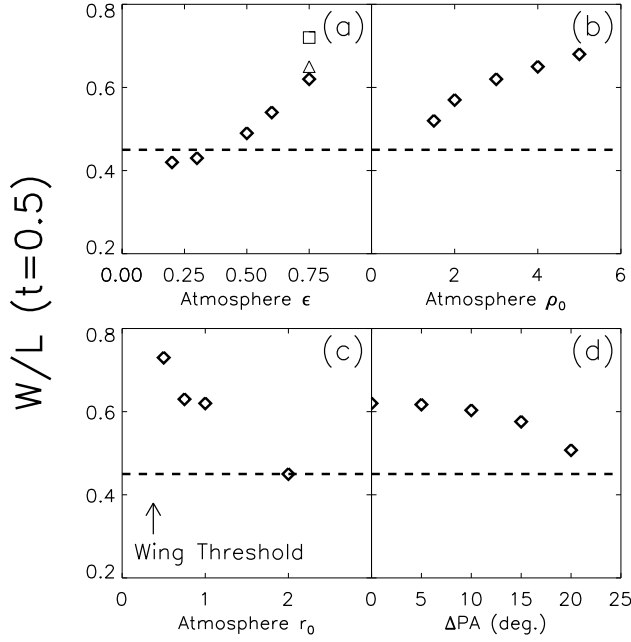


Figure 7. These plots show the dependence of axial ratio W/L on (a) the ellipticity of the atmosphere ϵ , (b) the core density ρ_0 , (c) the core radius r_0 , and (d) the angle between the jet and the major axis ΔPA . Each plot represents varying one parameter while holding the other standard atmosphere parameters ($\epsilon = 0.75$, $\rho_0 = 3.0$, $r_0 = 1.0$, and $\Delta PA = 0$) steady and using the standard jet. In panel (a) the square and triangle represent runs with different ϵ_x for $\epsilon_z = 0.75$, demonstrating the effect of triaxiality on W/L (Table 1). W/L is measured at $t = 0.5$ for all cases; for the standard jet, this represents the transition during the active phase from a powerful to a weak jet (this time and the “wing threshold” vary with choice of jet). Values taken from Table 1.

proceeds to a code time of 1.0, at which point the radio galaxy is in the early passive phase. Unsurprisingly, this run produces some of the most prominent wings of our suite (Figure 6); the shallow pressure gradient along the z -axis and declining velocity profile combine to produce stalled lobes which begin to collapse at the end of the active phase. At the same time, wings quickly escape the core region, and by $t = 0.4$ are easily recognizable (right-hand panels of Figure 2.2). After reaching $W/L = 0.83$ at $t = 0.75$, the cocoon collapse leaves the wings as the most notable features (Figure 5).

At $t = 1.0$, we re-inject a jet with $v_{\text{jet}} = 100c_s \exp[3(t - 1.0)]$ (Figure 5 and bottom panel of Figure 2.2). Since the jet is expanding into tenuous material from the old cocoon, the expansion quickly re-establishes a cocoon. However, the reinjection also drives a bow shock inside the collapsing cocoon, allowing initially strong back-flows to feed the wings directly. Hence, between $t = 1.10$ and $t = 1.35$, an X-shaped radio galaxy is apparent ($W/L \sim 1.2$). After $t = 1.35$, the jet again weakens to the point where collapse begins. If the jet is instead reinjected at the inception of the passive phase at $t \sim 0.75$, the end result is very similar ($W/L \sim 1.2$ at $t = 0.95$).

The atmosphere in this run is similar to the 2D simulations presented in Capetti et al. (2002) and 3D simulations in Zanni et al. (2003). Striking asymmetries develop despite the axisymmetric atmosphere because of turbulent mixing between different slices in ϕ and be-

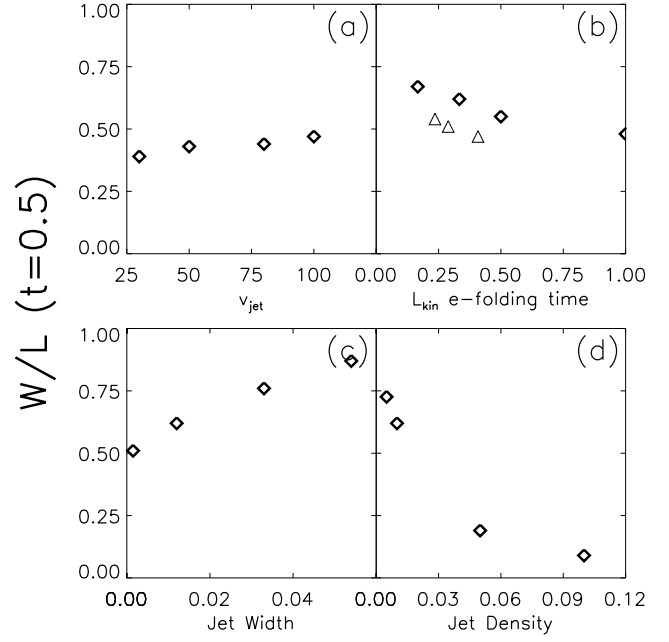


Figure 8. These plots show the dependence of axial ratio W/L on (a) jet velocity for a constant-velocity jet, (b) e-folding time for a decaying jet (diamonds represent jets of the form $v_{\text{jet}} = 100 \exp[-at]$ and triangles $v_{\text{jet}} = 100 \exp[-at^2]$), (c) area of the jet nozzle, and (d) density of the jet material. All runs are conducted in the standard atmosphere (Table 1). In (a) and (b), the jet kinetic luminosity is *not* conserved between runs, whereas in (c) and (d) we adjust the initial velocity v_0 to conserve L_{kin} . As in Figure 7, we show W/L as measured at a code time $t = 0.5$; all sources are in the active phase but not at the same place.

cause the back-flows form three-dimensional structures within the lobes. If these flows are slightly misaligned on opposite sides of the midplane, asymmetries develop.

Atmosphere— In our exploration of different atmosphere properties (Figure 7; Table 1), we vary ϵ , ρ_0 , r_0 , and ΔPA individually while keeping the other atmosphere parameters steady and using the standard jet ($v_{\text{jet}} = 100c_s \exp[-3t]$, $\rho_{\text{jet}} = 0.01$, $\alpha = \pi/35$, and $\beta = \pi/15$). Except when we vary ΔPA , the jet is coaligned with the major axis.

It is clear from Figure 7 that wing prominence depends strongly on the core radius r_0 , core density ρ_0 , and ellipticity ϵ . Because the lobes and wings evolve almost independently, these dependencies can be understood by breaking the axial ratio W/L into its constituent parts: the wing length W and lobe length L . For the purposes of this discussion, W and L are both taken to be measured at $t = 0.5$ (Table 1).

We find that L varies only slightly as a function of r_0 (less than 10%) but does peak between $r_0 = 0.5$ and $r_0 = 2.0$. At very low r_0 , the lobes are not confined by the atmosphere and spread out laterally, causing more turbulent mixing and dissipating the thrust of the jet. At very high r_0 , the lobes are completely confined by the atmosphere and the density gradient is so shallow that as the jet weakens it is increasingly resisted by the atmosphere. The importance of this effect on the lobes is more pronounced in a comparison between L and ρ_0 where the lobe length declines by 50% between $\rho_0 = 1.5$

and $\rho_0 = 5.0$.

On the other hand, the wing length W depends much more strongly on the core radius r_0 (declining precipitously with increasing r_0) and only weakly on the core density. This behavior occurs because the wings respond primarily to the pressure gradient along the minor axis (Equation 12) which depends on r_0 and ρ_0 as $\nabla P \propto \rho_0 r_0^{-2}$. Thus, a large W/L requires small, dense atmospheres.

In this context, the importance of ellipticity is clear: ϵ determines the ratio of core radii along the major and minor axes. For high ϵ , the lobes expand into material which does not vary much in density during the active phase whereas the wings quickly escape the core region. This behavior is unsurprising; Capetti et al. (2002) and Kraft et al. (2005) make the same basic argument for wings produced when the jet is coaligned with the major axis of the atmosphere. However, the interplay between the parameters rules out predicting the wing length from first principles. For instance, one might imagine that we could produce wings in an atmosphere with $\epsilon \sim 0.3$ (Figure 7) by making r_0 tiny and ρ_0 large. Although this *does* increase the wing length, the radio galaxy expands beyond the dense part of the atmosphere during the ignition phase so the jet does not face as much resistance as might be expected.

It is possible to produce wings in atmospheres with smaller ϵ by making the atmospheres triaxial (using prolate ellipsoids) instead of axisymmetric. Zanni et al. (2003) expect triaxial atmospheres (as opposed to the axisymmetric simulations of Capetti et al. 2002) to produce longer wings because the backflow is collimated along a single minor axis as opposed to forming a torus at the midplane. We find that while a triaxial atmosphere does collimate the wings, it does not by itself make them substantially longer relative to an axisymmetric atmosphere with the same maximum ϵ because the backflow in our simulations is a compressible fluid and wing growth is driven by buoyancy (the pressure gradient is the same along the minor axis). Rather, triaxial atmospheres produce better-defined proto-wing channels during the ignition phase. These channels are then reinforced during the active phase. In other words, triaxiality increases $W/L_{0.5}$ at smaller values of ϵ because the ignition cocoon is less axisymmetric.

Finally, we test the sensitivity of wing formation to the degree of alignment between the jet and major axis ΔPA (Figure 7d). Long wings are difficult to produce when the jet is misaligned with the major axis, and the wings produced differ in character. This is because the ignition cocoon produces proto-wings perpendicular to the jet instead of along the atmosphere's minor axis. Therefore, the longer wings which develop during the active phase do not benefit as much from the initial supersonic expansion. Wings also become increasingly associated with the lobe on their side of the major axis as ΔPA increases because the lobes are bent by the atmosphere and the back-flows no longer make it all the way to the midplane before flowing into the wings. Hence, the lobe-wing pairs are mirror-symmetric about the midplane. The angle between the lobe and the wing in each pair is also largely determined by ΔPA .

Table 2
Varying the Jet in the Standard Atmosphere

Name	Wings?	ρ_{jet}	$v_{\text{jet}}(t)/c_s$	α	β	W/L ($t = 0.5$)
Standard Jet						
STANDARD	Y	0.01	$100 \exp[-3t]$	$\pi/35$	$\pi/15$	0.62
Velocity Profiles						
SA_V30	N	0.01	30	$\pi/35$	$\pi/15$	0.39
SA_V50	Y	0.01	50	$\pi/35$	$\pi/15$	0.43
SA_V80	Y	0.01	80	$\pi/35$	$\pi/15$	0.44
SA_V100	Y	0.01	100	$\pi/35$	$\pi/15$	0.47
SA_VE1	Y	0.01	$100 \exp[-t]$	$\pi/35$	$\pi/15$	0.48
SA_VE6	Y	0.01	$100 \exp[-6t]$	$\pi/35$	$\pi/15$	0.67
SA_VG3	Y	0.01	$100 \exp[-3t^2]$	$\pi/35$	$\pi/15$	0.47
SA_VG6	Y	0.01	$100 \exp[-6t^2]$	$\pi/35$	$\pi/15$	0.51
Jet Density						
SA_D0.005	Y	0.005	$100f \exp[-3t]$	$\pi/35$	$\pi/15$	0.73
SA_D0.05	N	0.05	$100f \exp[-3t]$	$\pi/35$	$\pi/15$	0.19
SA_D0.10	N	0.10	$100f \exp[-3t]$	$\pi/35$	$\pi/15$	0.09
Jet Width						
SA_B30	Y	0.01	$100f \exp[-3t]$	$\pi/35$	$\pi/30$	0.51
SA_B7.5	Y	0.01	$100f \exp[-3t]$	$\pi/35$	$\pi/7.5$	0.76
SA_B5.0	Y	0.01	$100f \exp[-3t]$	$\pi/35$	$\pi/5.0$	0.87

Note. — The standard atmosphere is a relaxed, isothermal β -model with core radius $r_0 = 1.0$, core density $\rho_0 = 3.0$, ellipticity $\epsilon = 0.75$, and with the jet oriented along the major axis. Few runs are needed to deduce the dependence of the morphology on jet parameters other than the kinetic luminosity as a function of time, but in these cases we vary v_0 by some factor f such that $L_{\text{kin}}(t)$ is the same as in the standard atmosphere; see text for caveats of this approach.

Jet— In contrast to the atmosphere parameter exploration, determining the dependence of $W/L_{0.5}$ on the character of the jet is difficult because of the potential for time dependence in the jet power. This time dependence, along with the small width of the jets, also makes it more difficult to test our findings observationally. We insist that the jets be light, hypersonic flows (Section 2) which produce sources which resemble double-lobed radio galaxies, and within these constraints test the dependence of $W/L_{0.5}$ on jet power as a function of time, jet width, and density of jet material (Figure 8). For each of the simulations in Figure 8 we use the standard atmosphere with $r_0 = 1.0$, $\rho_0 = 3.0$, $\epsilon = 0.75$, and $\Delta\text{PA} = 0.0^\circ$. Note that Figures 8a and Figures 8b do *not* conserve kinetic luminosity between runs, whereas Figures 8c and Figures 8d do. The exploration of jet velocity is conducted with jets with the standard width of $\beta = \pi/15$ (~ 0.01 code units wide) and density of $\rho_{\text{jet}} = 0.01$.

Figures 8a and 8b demonstrate the importance of decaying jets to long wings. In Figure 8a, we use jets with differing velocities but no time dependence, finding that none produce a large $W/L_{0.5}$. $W/L_{0.5}$ actually *increases* with increasing v_{jet} even though the faster jets also punch through the atmosphere more quickly. This is because the overpressured cocoon produced by a weaker jet during the ignition phase is less overpressured and thus produces smaller proto-wings. Below $v_{\text{jet}} \sim 20c_s$,

the sources are not cocoon-bounded at all. Since the jets do not decay, W/L obviously decreases with time.

Powerful jets which decay (Figure 8b) are effective at producing wings because the proto-wings form during the ignition phase and the jet generates strong back-flows early on when the jet head is close to the midplane. Since the lobes grow increasingly slowly, the subsonically expanding wings keep pace with the active lobes more easily. As is clear in Figure 8b, the slower the decay, the smaller $W/L_{0.5}$ (diamonds represent exponentially decaying jets and triangles jets with $v_{\text{jet}} = v_0 \exp[-at^2]$). Jets with *increasing* velocity do not produce long wings because a powerful jet is necessary at the inception of activity to produce proto-wings.

In Figures 8c and Figures 8d we investigate the dependence of $W/L_{0.5}$ on jet width and density. We vary β and ρ_{jet} while conserving L_{kin} by varying the initial velocity of the jet v_0 , using the standard form of $v_{\text{jet}} = v_0 \exp[-3t]$. We limit these runs to those with v_0 capable of producing an overpressured cocoon that seeds proto-wings.

The nozzle width of the jet clearly has a strong effect on $W/L_{0.5}$ (Figure 8c). Increasing the jet width makes the ignition cocoon larger and more overpressured during the ignition phase, promoting expansion along the minor axis. The lobe width during the active phase increases with increasing β , dissipating the jet thrust over a larger solid angle. Short, fat lobes attached to fat wings result. On the other hand, if β is tiny, the jet drills through the surrounding atmosphere quickly, and thin, long lobes result. It is not clear whether jet widths actually vary substantially between sources and what determines the width of the jet; all jets are very narrow. Thus, our results are more generally a statement that jets which dissipate their thrust over a wider area produce longer wings.

Figure 8d shows $W/L_{0.5}$ as a function of ρ_{jet} . The sharp decline with increasing ρ_{jet} is due to the thrust carried by the jet. Even at moderate velocities, denser material drives the lobes forward much faster than light material while at the same time driving weaker back-flows. Hence, wing formation is not favored. We note that when $\rho_{\text{jet}} > 0.05$, the sound speed of the lobe material is not much greater than that of the ambient medium and the jet does not develop the usual KH instabilities. These jets are therefore not “light” as required to reproduce realistic radio sources with non-relativistic hydrodynamics (Section 2). However, these runs are shown along with the light ones to illustrate the importance of dissipating jet thrust to long wings.

Synthesis Runs— We have used the insights gained from examining the dependence of wing prominence on various atmosphere and jet parameters to new runs with complex atmospheres and jets in an attempt to produce long, realistic wings. These simulations (listed in Table 3) are not a systematic exploration of any phenomenon. We offer a few brief observations here.

Triaxial atmospheres offer the best hope of making long wings at lower ϵ (e.g. Figure 6), but still cannot produce substantial wings in our simulations for $\epsilon \lesssim 0.45$. Several runs from a large suite of such simulations are listed in Table 3 with the prefix TX. Generally, they follow the same trends as described in above; the impor-

tance of both favorable atmosphere and jet parameters to wings is obvious in the simulation with $\epsilon_z = 0.45$ (TX_E45_D5.0.WIDE), where a wide, decaying jet in a small, dense atmosphere is required to produce wings comparable to that in the standard atmosphere at lower ellipticity. Embedded disks of hot material (i.e. a thick disk; runs DISK_VE1 and DISK_VE3), however, alleviate the problem, allowing prominent wings to grow in atmospheres with globally small ϵ . These disks are somewhat denser than the larger ISM, so the ignition cocoon effectively encounters a small, dense, highly elliptical atmosphere during the ignition stage. The disks are blown apart by the blast wave from the ignition stage and might not be observable once the radio galaxy has turned on.

In most of our models, the ignition stage occurs in a smooth, relaxed medium. In real galaxies, the ignition stage would occur in the galactic center where mergers, dynamical effects, and other phenomena associated with AGN can significantly disturb the ISM. We do not attempt to model real galaxies, but find that adding Kolmogorov spectrum turbulence to our atmospheres or small bar-like perturbations to the underlying gravitational potential near the nucleus does not have a large effect on the ignition stage. As long as there is a sufficient amount of ISM distributed around the nucleus, an overpressured cocoon can form. On the other hand, in runs where we begin with a weak jet of $v_{\text{jet}} = 20c_s$ (twice the sound speed of the lobe material), and no cocoon is formed, wings do not form (the SLOW_START runs in Table 3). The backflow model has difficulty producing wings when a weak AGN suddenly becomes more powerful because an overpressured cocoon only forms when the jet is completely confined by the atmosphere. These runs can, however, produce something akin to Z-shaped morphology by virtue of the lobes escaping the densest regions of the atmosphere before the powerful jet turns on.

We have briefly investigated the potential for gas-rich “stellar shells” from minor mergers located periodically along the major axis to produce wings (motivated by Gopal-Krishna & Wiita 2010). We use a simple model in which only the positive peaks of two-dimensional sine/sinc waves are added to the density of an underlying elliptical atmosphere; the center is cut out. The amplitudes are set at a maximum of ρ_0 . The shells do not significantly impact the formation of wings emanating from the center of the galaxy, although they do resist the jet, allowing for a higher W/L (the SHELL runs in Table 3). In the model of Gopal-Krishna & Wiita (2010), wings are instead produced near the site of the shell, and we cannot reproduce this. Obviously, these runs are not a thorough exploration of the effect of stellar shells, especially if they actually bend jets (in which case they are beyond the scope of our models).

Motivated by the importance of a reinjected jet (Section 3.1), we examine the role of rapid intermittency (runs INTERMITTENT in Table 3). By this we mean jets which experience multiple outbursts during the run and which are essentially in an “on” state or an “off” state. Generally, we find that rapid intermittency has the effect of suppressing wing formation and results in much more regular cocoons (in terms of their projected morphology) than single outbursts. On the other hand, ragged cocoons are produced by long periods of dead time. In

Table 3
Synthesis Runs

Name	r_0	ρ_0	ϵ_x	ϵ_z	ρ_{jet}	v_{jet}/c_s	α	β	W/L_{max}
Interpolation									
WIDE_VE1	1.5	4.0	0.0	0.75	0.01	100 exp $[-t]$	$\pi/90$	$\pi/7.5$	0.58
WIDE_VE3	1.5	4.0	0.0	0.75	0.01	100 exp $[-3t]$	$\pi/90$	$\pi/7.5$	0.73
TX_E75_VE1	1.0	3.0	0.375	0.75	0.01	100 exp $[-t]$	$\pi/90$	$\pi/7.5$	0.63
TX_E75_VE1_BIG	1.5	4.0	0.375	0.75	0.01	100 exp $[-t]$	$\pi/90$	$\pi/7.5$	0.68
(restart at $t = 1.0$)									0.78
TX_E75_VE1_B7.5	0.75	3.0	0.375	0.75	0.01	100 exp $[-t]$	$\pi/90$	$\pi/7.5$	1.02
TX_E75_VE3_B5.0	1.5	4.0	0.375	0.75	0.01	100 exp $[-3t]$	$\pi/90$	$\pi/5$	0.82
TX_E60	0.75	3.0	0.30	0.60	0.01	100 exp $[-t]$	$\pi/90$	$\pi/7.5$	0.44
TX_E60_WIDE	0.75	3.0	0.30	0.60	0.01	100 exp $[-t]$	$\pi/90$	$\pi/5$	0.67
(restart at $t = 1.0$)									0.97
TX_E60_D5.0	0.75	5.0	0.30	0.60	0.01	100 exp $[-t]$	$\pi/90$	$\pi/7.5$	0.71
TX_E45_D5.0_WIDE	0.75	5.0	0.225	0.45	0.01	100 exp $[-3t]$	$\pi/90$	$\pi/5$	0.58
Other									
DISK_VE1	2.0	3.0	0.25	0.50	0.01	100 exp $[-t]$	$\pi/90$	$\pi/7.5$	0.60
	0.25	8.0	0.0	0.90					
DISK_VE3	2.0	3.0	0.25	0.50	0.01	100 exp $[-3t]$	$\pi/90$	$\pi/7.5$	0.83
	0.25	8.0	0.0	0.90					
TURBULENT ^a	1.0	3.0	0.0	0.75	0.01	100 exp $[-3t]$	$\pi/90$	$\pi/7.5$	0.64
SHELL_VE1 ^b	1.0	3.0	0.0	0.75	0.01	100 exp $[-t]$	$\pi/90$	$\pi/7.5$	0.53
SHELL_VE3 ^b	1.0	3.0	0.0	0.75	0.01	100 exp $[-3t]$	$\pi/90$	$\pi/7.5$	0.71
INTERMITTENT	2.0	2.0	0.0	0.75	0.01	100 sin ² $[50t]$	$\pi/90$	$\pi/7.5$	0.44
INTERMITTENT2	1.0	3.0	0.0	0.75	0.01	100 sin ² $[6t]$	$\pi/90$	$\pi/7.5$	0.47
SLOW_START_1 ^c	1.0	1.5	0.0	0.75	0.01	20 <i>to</i>	$\pi/90$	$\pi/7.5$	0.42
						100 exp $[-t]$			
SLOW_START_2 ^c	1.0	1.5	0.0	0.75	0.01	20 <i>to</i>	$\pi/90$	$\pi/5$	0.45
						100 exp $[-t]$			
SLOW_START_3 ^c	1.0	5.0	0.0	0.75	0.01	20 <i>to</i>	$\pi/90$	$\pi/5$	0.55
						100 exp $[-t]$			

Note. — A representative sample of our non-systematic exploration of parameter space; not all runs attempted are included. “Interpolation” runs refer to those runs which are a natural extension of Tables 1 and 2 whereas “other” runs include substantially different atmospheres and jet behaviors. See text in Section 3.2 for discussion.

^a This is the standard run with axisymmetric Kolmogorov spectrum density perturbations introduced to the atmosphere.

^b Shells of material with a peak amplitude $\rho = 3.0$ were superimposed on the standard atmosphere; shells are generated along the z -axis by using 2D sine or sinc functions with a period of $z \sim 0.5$.

^c $v_{\text{jet}} = 20c_s$ from $t = 0.0$ to $t = 0.25$ and $v_{\text{jet}} = 100 \exp[-(t - 0.25)]$ thereafter.

neither case are wings promoted, as each successive brief outburst deposits most of its thrust at the ends of the lobes, far from the midplane. The chief reason why such intermittency does not produce prominent wings is that wings expand subsonically. Since the duty cycles of the intermittent jets are much shorter than the crossing time, the cocoon expands as if a moderately powerful jet of constant velocity were powering it. Unlike in single decaying outbursts, the intermittent jets deposit most of their thrust far from the midplane. On the other hand, intermittency on the timescale of an e -folding time of a decaying jet can be effective.

4. SIMULATION LIMITATIONS

Because we have only solved the equations of hydrodynamics in evolving our simple models, it is worth considering the impact of additional complexity.

4.1. Missing Physics

Our models do not include magnetic fields, special relativity, or radiative losses, and our simple setup does not take into account complex jet or atmospheric structure, feedback, and other processes that may be important to radio galaxy morphology. In practice, we do not believe

these omissions invalidate our results. For example, special relativity and magnetic fields must play crucial roles in determining the character and transverse structure of the jet, but we only insist that our simulated jets reproduce the collimation, hot spots, and back-flows of FR II sources. In other respects (e.g. radiative efficiency), the jet and AGN are inside a “black box.” Because we are concerned with the behavior of lobe material, we believe these omissions are justified.

Likewise, radiative losses (depleting of lobe energy via synchrotron emission and inverse Compton scattering) only become important relative to adiabatic losses at late times and are not in a position to influence the formation of wings. Radiative losses from the ICM are also irrelevant on the timescales of AGN outbursts, so feedback (the connection of jet power to the amount of material crossing the inner boundary) resulting from cluster cooling is unimportant on these timescales. As to feedback from *backflow* (Antonuccio-Delogu & Silk 2010), there is no obvious recipe to describe what happens to the mass flowing across the inner boundary, since the inner boundary radius is much larger than the nuclear engine, but as the back-flows straighten, less material will have velocity vectors pointing towards the origin and eventually

the AGN would cease to be “fed” by backflow. This is consistent with our entirely artificial recipe for decaying jets.

On the other hand, magnetic fields (that must be injected with the jet) and relativistic jets (which have a higher thrust for a given mass-energy density) may strongly influence the behavior of lobe material.

Toroidal magnetic fields may help collimate the backflow and retard its mixing (e.g. Braithwaite 2010). The apparent continuity of fields in some wings (e.g. NGC 326 in Murgia et al. 2001) is suggestive, especially considering that in our models the lack of collimation leads to wide wings. However, Huarte-Espinosa et al. (2010) find in simulations of FR II sources that turbulence sets in within the cocoon even when ordered fields existed earlier, so it is unclear that the magnetic fields in the wings are actually toroidal. As to the realism of the *jet*, it is not our goal to understand the jet physics in detail, but we note the persistence of experimental hypersonic fluid jets in recent work by Belan et al. (2011), which the authors use to argue that magnetic collimation is only required near the base of the jet.

The importance of relativistic jets to the cocoon morphology is unclear. Komissarov & Falle (1996) find that, for jets matched by velocity, pressure, radius and power, relativistic jets produce preferentially wider cocoons than classical ones. The authors suggest that this effect may be accounted for by the higher thrust in the relativistic case. However, Rosen et al. (1999) find the opposite when using the same matching conditions: relativistic jets tend to produce narrower cocoons compared to classical jets (more specifically, jets with a higher Lorentz factor have smaller cocoons). Without matched relativistic simulations it is impossible to directly test the importance of special relativity on our cocoon sizes, but it is remarkable that Rosen et al. (1999) and Komissarov & Falle (1996) agree that the qualitative nature of the cocoon is unchanged. Including relativity may modify W/L but would not fundamentally change the appearance of our winged sources because relativistic physics in the lobes would not change the processes which produce wings. In other words, we believe that special relativity is a second-order effect akin to magnetic fields.

4.2. Initial Conditions

It is worth asking whether wings form only because our atmospheres are “smooth”, i.e. because we have not included turbulence in the ICM or structure near the center (where the environment is presumably complex). This question is particularly important given the observed interactions between jets and molecular clouds (e.g. Ly et al. 2005), stellar shells (e.g. Gopal-Krishna & Wiita 2010), gas in companion galaxies (Evans et al. 2008), and more generally the complex nuclear environments of active galaxies (e.g. Rosario et al. 2010). To this end, we have introduced density perturbations mimicking stellar shells along the major axis at various intervals, tested the impact of a single ring near the nucleus, and introduced Kolmogorov-spectrum turbulence to the ICM. None of these structures alter the same basic evolution of winged sources. Additional jet physics would need to be in place in order to determine whether the jet itself can be bent by interaction with high density pockets (Gopal-Krishna & Wiita 2010). All

of these tests use density perturbations with a maximum amplitude of the core density ρ_0 . Finally, bulk flows in clusters are clearly important to radio galaxy structure (Morsony et al. 2010), although most XRGs are large, strongly bridged sources in which this may not be a defining effect.

4.3. Artifacts

It is encouraging that our simulated radio galaxies reproduce the basic features of other simulations in the literature (e.g. Reynolds et al. 2002; Heinz et al. 2006; Vernaleo & Reynolds 2007; Antonuccio-Delogu & Silk 2010), but it is worth considering the impact of boundary conditions and the jet structure on the morphology of the lobes—our setup is designed to produce lobes like those of radio galaxies with physics and conditions inherently different from those encountered in nature. The mixing experienced by the lobes is also artificial (naturally set by the size of the grid zones, which vary along r and θ), but mixing is too slow a process to suppress the formation of wings.

The inner boundary is the most significant artifact of our simulation because it represents no physical analog but rather allows us to hide the AGN and the jet collimation mechanism. In addition, backflow crossing the boundary slows down and disappears. This has two consequences: not all the backflow can be harnessed, and flows may be effectively directed around the boundary by eddies as slowing backflow crosses the boundary. In the first case, the amount of material is too small to influence the wings. In the second, we find that the inner boundary must be small compared to r_0 (keeping the physical size of the jets fixed) in order to prevent the initial cocoon from being unduly influenced by the sphere. Inner boundary spheres which are too large tend to promote material flowing around them, hence promoting early wings, but suppress midplane mergers and hence the prominence of later wings. The initial interstices also survive for longer for oversized r_{inner} . For typical atmospheres ($0.5 < r_0 < 1.0$), r_{inner} must be somewhat smaller than 0.1 code units; $r_{\text{inner}} = 0.05$ is a compromise between a small impact on the initial cocoon and reasonably sized grid zones. Runs with $r_{\text{inner}} = 0.01$ do not appear substantially different from those with $r_{\text{inner}} = 0.05$, and the timestep is unreasonably small.

We precess the jet injection footpoints rapidly (20π Hz) in a very tight circle around the poles in order to break up the jet symmetry and spread its thrust out over a larger working surface. We only require that our jet reproduce internal features seen in other hydrodynamic simulations along with the terminal shocks that give rise to the backflows and lobes. Without breaking up the jets, the jet head travels very quickly and produces unrealistic lobes (e.g. Vernaleo & Reynolds 2006); in MHD simulations we would expect helical instabilities to break up the jet. Our precession scheme is thus an artifice that is motivated by observables but whose recipe is not an attempt to model a physical process (c.f. Heinz et al. 2006). However, one might worry about its influence on backflow and wings because the precession angle is a free parameter (subject to the condition that $\alpha < \theta_{\text{jet}}$). In other words, we can tune the width of the lobes and the rate of growth of the radio galaxy within some narrow range of parameters. Since stalling the jet head contributes to wing promi-

nence via shortening the active lobes, is the axial ratio W/L artificially high? We do not believe so. Even with tiny precession angles, we form long wings in highly eccentric atmospheres (the only atmospheres where long wings form). Moreover, the jet head advance speed also depends on the kinetic luminosity as a function of time.

5. PROPERTIES AND PREDICTIONS OF THE BACKFLOW MODEL

We have successfully produced winged and X-shaped sources solely by redirecting back-flow with static environmental pressure gradients, and are now in a position to compare our simulated sources to observed XRGs (Figure 11) in order to critique proposed wing formation mechanisms involving back-flows. In these models, wings are produced as plasma flowing back from the jet heads is deflected into a direction misaligned with the jets. How this deflection occurs is uncertain (Leahy & Williams 1984; Worrall et al. 1995; Capetti et al. 2002; Kraft et al. 2005; Gopal-Krishna & Wiita 2010), and until now the backflow model has not been rigorously investigated with three-dimensional simulations.

Here we outline a series of predictions (expectations) for properties which are, at least in principle, observable if our simulations are an adequate representation of wing formation. These predictions are also summarized in Table 4. We then assess the backflow model in light of these predictions and briefly discuss the implications of our work for the wider sample of distortions to the canonical double-lobed morphology of bridged radio galaxies.

5.1. Predictions

X-shaped and winged sources are one family— The most natural consequence of the backflow model is that short and long wings are produced in the same way. Short wings should then be more common than long ones since the long wings are harder to produce. Although this is an obvious point, we note it as a potential observational test because sources with shorter wings and the candidate X-shaped sources (Cheung 2007) have not been tested for several of the trends seen in XRGs (most importantly, the jet-major axis correlation Capetti et al. 2002; Saripalli & Subrahmanyan 2009). Our simulated sources predict that winged sources will fall in line, albeit with a greater spread in parameter space.

Projection almost always enhances W/L — Wings in our models (even those produced by triaxial atmospheres) tend to be wider than the lobes and hold their shape better in rotation and projection. Hence, we predict that projection almost always enhances W/L . In other words, some observed sources with high W/L_{obs} probably have an intrinsically smaller aspect ratio (e.g. Figure 11). If the projection angle can be worked out for a sufficient number of XRGs and winged sources, we expect the lobes in a number of XRGs to be shortened via projection, i.e. the intrinsic distribution of W/L is shifted from the observed distribution (an idea of the observed distribution may be found in Saripalli & Subrahmanyan 2009). If this does not turn out to be the case, the backflow model would need a collimation mechanism (see subsonic expansion below) to be consistent with observations. Un-

fortunately, this prediction makes it difficult to quantitatively compare the simulated population to the observed on because in most XRGs the projection angle is unknown.

Long wings require high ellipticity— Our simulations predict that intrinsically long wings can only be produced in very elliptical atmospheres (Figure 7). The lowest ϵ for which we can make convincing wings is $\epsilon \sim 0.45$, and very long wings require $\epsilon > 0.55$. These values are much higher than the average powerful radio galaxy host ($\epsilon_{\text{peak}} \sim 0.2$; Smith & Heckman 1989) and even most XRGs. A high initial atmospheric ellipticity (or higher order asymmetry) is a clear prediction of our models, but confirming this behavior in observed sources is difficult.

For instance, a few sources with very small host ϵ and large W/L (the best example is NGC 326) appear to have wings originating *outside* the ISM, so it is not evident that the ellipticity of the ISM is always the relevant value for comparison. Further, the ellipticity of the ISM may differ substantially from that of the host galaxy on small scales (Diehl & Statler 2007) even when in broad agreement on galactic scales (Hodges-Kluck et al. 2010). In this case, the best example in the literature is 3C 403 (Figure 1, where $\epsilon_{\text{ISM}} = 0.059$ and $\epsilon_{\text{optical}} = 0.25$ (Kraft et al. 2005)). Indeed, we find that elliptical atmospheres of moderate ϵ with embedded disks are as effective at producing wings as single-component atmospheres with extreme ϵ , but the disks are largely destroyed by the radio galaxy. High resolution imaging may be required to see any disk remnants. The triaxiality of elliptical galaxies also plays a role, since we may not measure a true ellipticity. Finally, because projection tends to enhance W/L , extreme values of $\epsilon \sim 0.75$ (as we use in the standard atmosphere) are not required to produce observed long wings. All else being equal, we still expect the intrinsic W/L to be correlated with ϵ , but the caveats outlined above make it a difficult proposal to test presently.

Wings require a jet pointed nearly along the major axis of an anisotropic environment ($\Delta\text{PA} \sim 0$)— As expected (based on the studies in Capetti et al. 2002; Saripalli & Subrahmanyan 2009; Hodges-Kluck et al. 2010), wings require a strongly asymmetric environment in which the jet is stalled by progression along the long axis (Figure 7). The wings grow in the favorable pressure gradients along the minor axis or axes. Our models expect a fairly strict requirement for the jet to be within $\sim 15^\circ$ of the major axis for substantial wings to be produced via the overpressured cocoon channel (the usual method for seeding wings in our models). The requirement is even more stringent in the event that a disk is present, indicating that disks are likely to be important only in a minority of cases.

As ΔPA increases, the wings become shorter (Figure 7) as well as increasingly associated with the lobe on the same side of the major axis. These lobe-wing pairs thus have mirror symmetry about the midplane. This is in agreement with radio maps of such sources. Since wings long enough to qualify the source as “winged” can be produced for a $\sim 15^\circ$ range of major axis–jet separation and truly X-shaped sources are only (intrinsically) produced for $\Delta\text{PA} < 5^\circ$, we would expect $\sim 2/3$ of winged sources

Table 4
Model Predictions

	Expectation	Observed?	Reference
1.	Short wings common; (intrinsically) long wings rare	No in SS09 sample (yes including C07?)	SS09
2.	Projection tends to enhance W/L	Undetermined	
3.	W/L correlated with ϵ_{ISM} (weaker correlation with host ϵ)	Sample size too small	HK10
4.	Wings require a jet aligned near the major axis	No?	C02,SS09
5.	W/L enhanced by higher pressure, small atmospheres	Yes	C02,SS09,HK10
6.	Most XRGs should be weak FR IIs (and hence strongly bridged sources)	Yes?	L10
7.	Intermittency on scales of 3–10 Myr produces longer wings	Yes?	SS09
8.	Wings are fainter than lobes	Yes	C09,L10
9.	Wings have flat spectral indices	Yes	LW84
10.	Backflow follows existing channels (collimation requires existing channels)	Undetermined	
11.	Wings grow subsonically (hence wing AGN outbursts are old)	Yes	LW84
12.	Flow speeds in wings should be transonic for lobe material	Mixed results	LR07
		Yes?	SS09
	Backflow model piggybacks on other hydrodynamic models	Yes?	SS09

References. — C02: Capetti et al. (2002); C07: Cheung (2007); C09: Cheung et al. (2009); DT02: Dennett-Thorpe et al. (2002); HK10: Hodges-Kluck et al. (2010); L10: Landt et al. (2010); LW84: Leahy & Williams (1984); LR07: Lal & Rao (2007); SS09: Saripalli & Subrahmanyan (2009)

Note. — Predictions for XRG properties if our model is accurate; note that these may not hold for the “backflow model” generally as phrased in prior work. Predictions correspond to arguments made in Section 4.

to have lobe-wing pairs, with acute angles between a lobe and its wing produced for smaller angles and obtuse angles for larger ones. Thus, we suggest that the existence of a large number of sources with lobe-wing pairs rather than true X-shaped morphology is consistent with the backflow model. However, we would also expect that wing length would decrease with increasing ΔPA ; this has not yet been measured.

Longer wings are produced in higher pressure, smaller atmospheres— Steeper pressure gradients occur for smaller core radius and higher core density/pressure (Equation 12). Since the steepness of the pressure gradient influences the rate at which wings grow, these small, dense atmospheres (e.g. the ISM) are better at producing wings. Moreover, wings can only form via the overpressured cocoon channel if the cocoon can escape the central core region and its high density before it comes into pressure equilibrium. The top panels of Figure 2.2 demonstrate this point (see also Figure 7). Finally, a high core density also resists the jet advance along the major axis, allowing the wings to grow longer. Thus, our models expect that the hosts of XRGs (where the jet is presumably pointed along the major axis) have higher pressure, on average, than those normal radio galaxies with jet geometry favorable to wings. Landt et al. (2010) find that the nuclear regions of XRGs have high temperatures ($T \sim 15000$ K) indicating that these regions may be overpressured. Although this does not directly correspond to our models of relaxed, isothermal atmospheres, our requirement for a small, high pressure environment is in agreement with their work.

Most XRGs should be weak FR IIs— Another key ingredient in our models is a decaying jet that begins as a powerful FR II source and decays to luminosities more typical

of FR I sources. A powerful jet is required to produce the overpressured cocoon and drive wings early on, whereas once wings begin expanding subsonically, a weakening jet (which advances increasingly slowly along the major axis of the atmosphere) allows the wings to become quite prominent. If the atmosphere is much smaller than the radio galaxy (as in many cases), a decaying jet will still grow more and more slowly, allowing subsonically growing wings to keep up. This finding naturally explains the observations that XRG radio powers tend to lie near the FR I/II “break” (Cheung et al. 2009) while also possessing strong bridges associated with powerful FR II sources (Leahy & Williams 1984). Landt et al. (2010) argue that XRGs are the archetypal transition population between FR I and FR II sources, with about half the XRGs in their sample having weak emission lines from the AGN (weak-lined FR IIs are otherwise uncommon). This suggests that there is indeed an evolutionary progression in the AGN and jet luminosity of XRGs. Our models predict a fast-rise exponential-decay profile in which the XRG spends most of its lifetime as a weak FR II source (Figure 8). However, we note that Best (2009) find in an SDSS study that FR I and II sources are not as obviously separated as in Ledlow & Owen (1996) and that FR II morphology occurs for a variety of radio powers and host galaxy masses.

Intermittency is another important prediction of our models for observed XRGs, but the action of intermittency in our simulations may represent a more complex underlying process. Intermittency on timescales similar to the e -folding time of a decaying jet (near the early passive phase) is effective in our simulations because it allows the jet to bypass the overpressured cocoon stage and form a bow shock within the radio lobe itself, thereby depositing a large amount of backflow into the wings from

a very powerful jet close to the wing bases. Reinjection is effective in a relatively narrow window of time (3–10 Myr depending on the size of the radio galaxy, e.g. Figure 5) between the active and passive phases, but this may be plausible: the ripples in the Perseus cluster (Fabian et al. 2006) and Abell 2052 (Blanton et al. 2009) do imply an AGN duty cycle of about 10 Myr. This is consistent with our simulated sources between 50–100 kpc across. Thus, it is conceivable that regular intermittency is a viable mechanism for enhancing wings, although we note that if the intermittency is very rapid or very slow, it is ineffective (Section 3.2). On the other hand, intermittency could be replaced in our models by any mechanism which drives back-flows nearer the base of the wings such as the motion of denser ISM into the path of the jet. We note that intermittency may also be effective for wings attached to the primary lobes farther from the nucleus; a reinjected jet quickly re-establishes the cocoon and drives strong back-flows along its length as it rapidly reaches the prior hot spot. If the jet reinjected is similar to the outburst which initially formed the wings, we would still expect XRGs mostly to be weak FR II sources.

Wings should be fainter than the primary lobes— The active lobes of XRGs are typically brighter than the wings. This behavior persists at lower (MHz) frequencies and is therefore not obviously attributable to spectral ageing, although spectral ageing may be in play for some XRGs (Lal & Rao 2007). Our models expect the wings to be fainter because they are substantially wider than the collimated primary lobes yet contain (in most cases) less lobe material. We therefore suppose that the wing material spreads out and decreases the magnetic field energy density U_B .

Assuming that U_B decreases with increasing volume (i.e. assuming something like equipartition conditions, although precise equipartition is not required), the synchrotron emissivity in the wings will be substantially smaller than that in the lobes. In other words, “spherical” wings a factor of ~ 2 wider than the active lobes will have a factor of ~ 8 smaller U_B than in the lobes. In optically thin conditions (a good assumption), the surface brightness obtained from integrating through the wings only recovers a factor of ~ 2 in the wings, so we expect them to be a factor of ~ 4 dimmer than the active lobes (more generally, the square of the ratio between the wing width and the lobe width) for electrons of the same γ . Of course, in projection the wings may appear even dimmer since the lobes will tend to be shortened and therefore increase in surface brightness (ignoring relativistic dimming of the counterjet) whereas the wings will not.

Clearly, this prediction rests on a number of assumptions not included in our models and is therefore somewhat weak. Since the wings are filled with turbulent plasma, it is also possible that the magnetic field strength is increased by winding up of fields as the material mixes. Moreover, the jet power (and therefore the back-flow speed) is time dependent in our simulations, so the ratio between the surface brightness of the lobes and the wings would be time dependent in our model as well. Nonetheless, the diffusion of material in the wings and the aforementioned projection effects seem likely to dim the wings in the backflow model.

Backflow follows existing channels— Most of the wings in our simulated sources are seeded by the pressure-driven expansion of an overpressured cocoon early in the source’s life. This cocoon expands asymmetrically because of the asymmetric pressure gradients and forms proto-wings which are later bolstered by the merger of laminar back-flows near the midplane sending material into the wings during the active phase. The laminar back-flows themselves are ineffective at drilling new channels. During the overpressured phase they acquire a vorticity near the terminal shocks that leads them to follow the contact discontinuity of the cocoon and ultimately flow back towards the AGN (Figure 3). During the active phase, they are mostly straight and flow towards the midplane.

Lobe material is also ineffective at producing channels because it follows the path of least resistance: in a confined ellipsoidal cocoon, it will simply spread out to increase the pressure throughout the cocoon rather than break out in a particular direction. This can be seen in the false synchrotron maps in Figure 2.2. These maps assume equipartition and are not indicative of what the sources would look like in the GHz bands. Rather, they effectively trace pressure in the cocoon, and it is easy to see that the pressure in the confined cocoon on the left side of the figure remains high relative to the X-shaped source (the false radio maps use the same scale).

Apart from proto-wings produced by the early pressure-driven expansions, Kelvin-Helmholtz and Rayleigh-Taylor instabilities produce channels which backflow reinforces. Given sufficient time and a powerful jet, these whorls and fingers can become wings in their own right, but likewise this is due to the growth of the instabilities and buoyancy rather than redirected laminar back-flows.

Notably, some sources exhibit wings which do *not* emanate from the center or are unlikely to have been produced via an overpressured cocoon (e.g. NGC 326). Because it is difficult to channel the back-flows, we hypothesize that if the backflow model is correct, some seed proto-wing was necessary to produce such sources. The origin of these proto-wings is unclear.

Wings expand subsonically— Related to the expectation that back-flows are not directly responsible for drilling channels is the prediction that the wings of radio galaxies expand subsonically for most of their lifetimes (Figures 3 and 4). This expectation is contrary to the Capetti et al. (2002) “overpressured cocoon” and Worrall et al. (1995) or Leahy & Williams (1984) “buoyant backflow” proposals in the literature (Section 1) and poses a serious problem for the backflow model in terms of explaining long wings. We therefore discuss this point in some detail below.

The problem of subsonic expansion can be broken into two distinct objections: (1) If the wings grow subsonically while the primary lobes grow supersonically, how can wings be longer than the lobes? and (2) Subsonic expansion implies wing lifetimes of more than 100 Myr for sources hundreds of kpc across. The first objection is easier to reconcile with our models because our jets provide a natural mechanism for the subsonic expansion of the lobes, and it is not clear whether most radio galaxies (even powerful ones) really do expand very supersonically.

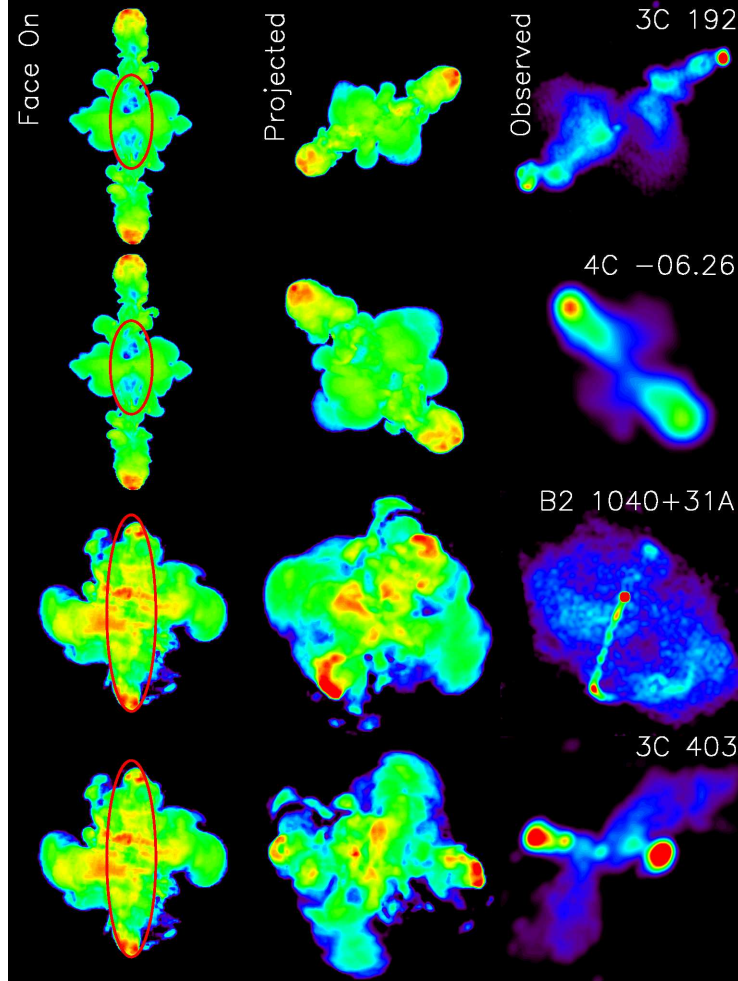


Figure 9. Gallery of false equipartition synchrotron maps ($j_\nu \propto p/\rho^{7/4}$) showing the resemblance between our winged sources and observed XRGs, and the importance of projection. Left: Face-on view showing intrinsic structure. The red ellipses show the core radius isobar of the model atmosphere. Center: Rotated and projected view. Right: XRG analog (various resolutions). We only show a few examples of simulations and note that any one simulation can reproduce several observed sources; more than 60 of the sources in Cheung (2007) can be plausibly reproduced by our simulations (in terms of appearance).

cally. Further, as we have noted, projection tends to enhance wings. However, the lifetimes of large sources are more difficult to explain.

To see this, consider that for a rich cluster atmosphere with $kT \sim 10$ keV (this corresponds to a $c_s \sim 1000$ km s $^{-1}$ or, conveniently, 1.0 kpc Myr $^{-1}$), subsonic growth implies that wings 100 kpc from base-to-tip would be at least 100 Myr old. In group environments, where $c_s \lesssim 500$ km s $^{-1}$ and monotonically declines at large radii (Sun et al. 2009), the longest observed wings (e.g. 3C 315 whose wings span ~ 400 kpc) could be almost 500 Myr old! Even if AGN activity persisted this long, synchrotron cooling might set in: if the bulk flows of replenishing backflow travel at a lobe sound speed $10c_s$, they would take between 20–100 Myr to replenish the leading edges of the wings. Depending on the break frequency and assuming magnetic fields in equipartition (B of a few μ G) and a Lorentz factor γ of several $\times 10^3$, this may easily exceed the radiative cooling time.

To solve this problem, variations of the backflow model require that the wings actually do expand supersonically. In the “overpressured cocoon” model (Capetti et al.

2002), supersonic wing growth is achieved through sustained pressure-driven expansion, whereas in the “buoyant backflow” model (Worrall et al. 1995), wings are driven by the nearly free expansion of diverted hyper-sonic back-flows. Our models reproduce overpressured cocoons and hypersonic back-flows, but the overall wing advance speed is subsonic.

For the overpressured cocoon model to produce long wings, a sustained overpressured state must be maintained to drive outflows. However, in our models the highly overpressured cocoon that forms soon after ignition quickly expands to reach pressure equilibrium: the supersonic expansion phase lasts at most around 15% of the lifetime of the radio galaxy regardless of the jet we inject (e.g. Figure 4). As the radius of the (isobaric) cocoon grows, its pressure falls much more rapidly than does that of the surrounding atmosphere at a similar radius (see also Zanni et al. 2003, Figure 2 in their paper), so the advance speed of the lateral cocoon expansion falls precipitously from a peak of about Mach 2. Thus, overpressured expansion appears to be relevant only very early in the life of the source and by

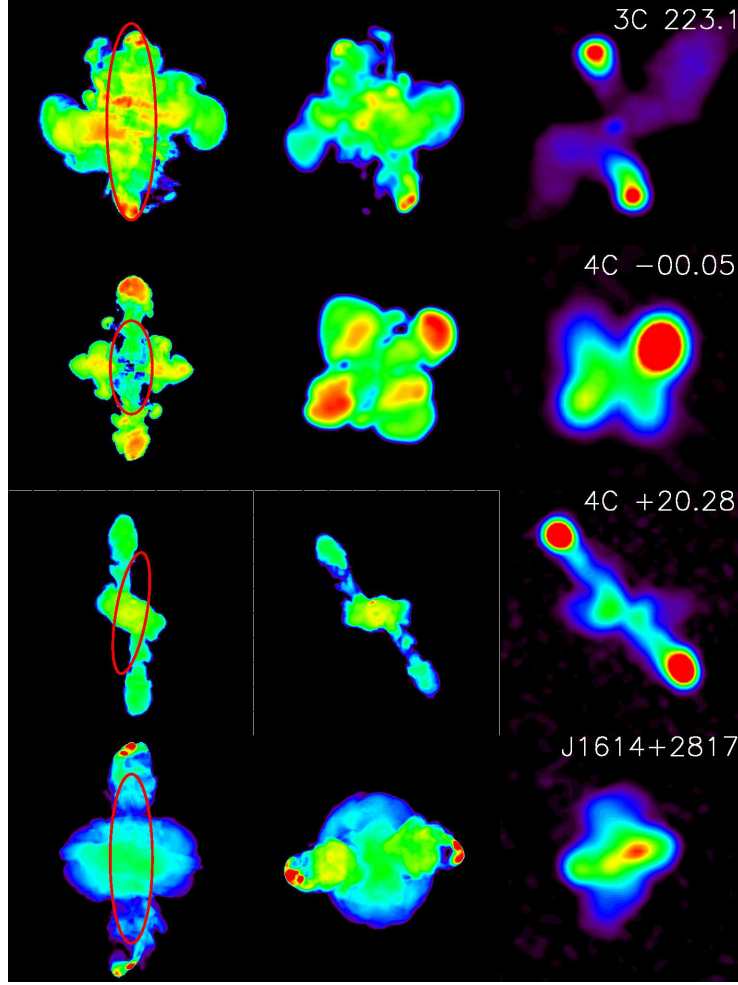


Figure 10. Figure 9 continued.

itself can produce only short wings. Indeed, this conclusion is supported by earlier simulations (Zanni et al. 2003) where even in advantageous triaxial atmospheres, the overpressured cocoon produced at most an intrinsic W/L of ~ 0.5 (the jets in their work were held at constant velocity and W/L would thus decrease over time). Saripalli & Subrahmanyan (2009) suggest that the overpressured state may instead result from backflow piling up upon reaching the central (dense) region of the galaxy. Our models do not support this scenario, since the cocoon is contiguous and nearly isobaric throughout the active phase.

The buoyant backflow model argues that a combination of buoyancy forces and wings driven by hypersonic flows produce large X-shaped sources. For instance, Dennett-Thorpe et al. (2002) estimate that the current outburst in 3C 403 (Figure 1) started 16 Myr ago. If this outburst was solely responsible for generating the ~ 100 kpc wings hydrodynamically (as preferred by Kraft et al. 2005), the average expansion speed of the wings would have to be $\sim 8000 \text{ km s}^{-1}$ ($0.027c$). In contrast, a typical sound speed for galaxy groups is $c_s \lesssim 500 \text{ km s}^{-1}$, a factor of 16 smaller. Likewise, Worrall et al. (1995) prefer hypersonic expansion. What could drive such wings? The answer invoked by these authors is redirected back-flows, which can be accel-

erated at the terminal hot spots up to a few percent of c (based on the spectral ageing–distance method of Alexander & Leahy 1987). The observational inference of high backflow speeds is consistent with our models and others (e.g. Antonuccio-Delogu & Silk 2010), which find back-flow speeds of about twice the lobe sound speed ($c_{s,\text{lobe}} = 10c_s$). Further, Saripalli & Subrahmanyan (2009) argue that the collimated morphologies of some wings requires some driving force.

However, it is not evident that these laminar back-flows can be harnessed to drive wing expansion (see the prior prediction). Subsonic wing growth in our simulations is a natural consequence of the tendency of backflow (lobe material) to mix and expand. The fast back-flows from the terminal shocks merge near the midplane, dissipating their speed and driving flows into the wings which are subsonic relative to the low-density material in the lobes (Figure 3), although they are still supersonic relative to the background. These flows then expand and decelerate further in the wings, dissipating their thrust over a very large area. Hence, detection of $10^3 - 10^4 \text{ km s}^{-1}$ flows in the wings would be insufficient evidence for hypersonic wing expansion. Supersonic wing expansion would require collimation to prevent thrust dissipation.

Can a collimation mechanism be found? An obvious possibility we have not included is ordered magnetic

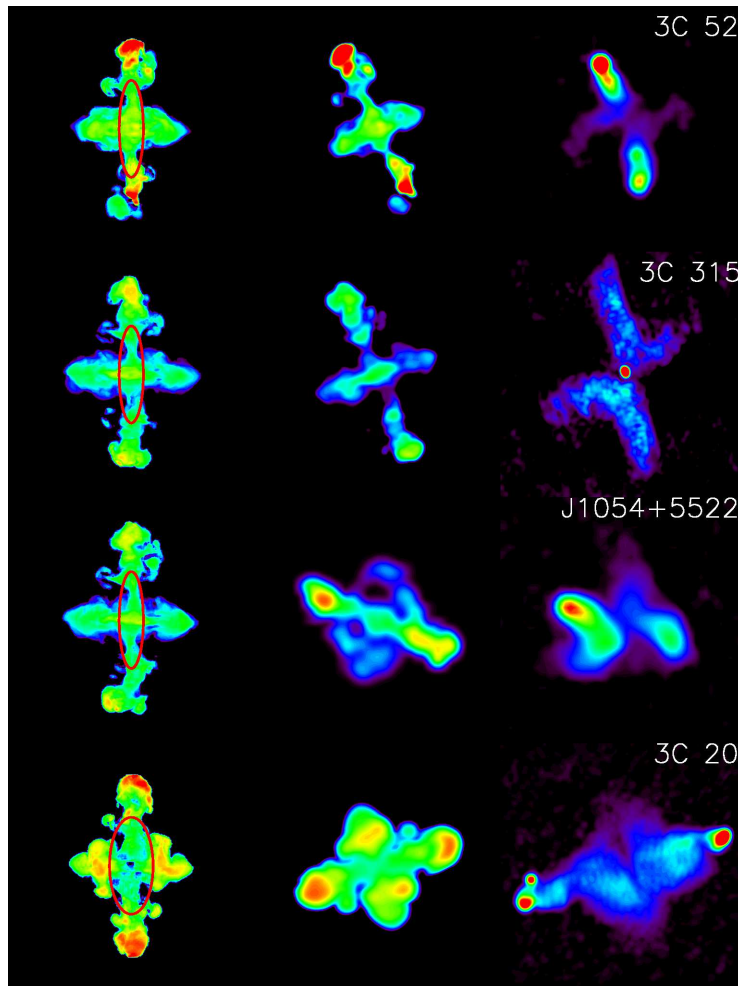


Figure 11. Figure 9 continued.

fields, since particles can move along them much more easily than across, but (Huarte-Espinosa et al. 2010) find that in FR II sources, lobe magnetic fields become turbulent on timescales of ~ 10 Myr. More generally, we note that (weak) shocks found around double-lobed radio sources often imply cocoon expansion near Mach 1. If a powerful jet cannot drive highly supersonic expansion, it seems unlikely that less powerful, more disorganized backflow could do so.

Lastly, it is important to emphasize that subsonic expansion is only a serious problem for very large wings or very young AGN with a large W/L ratio. Our simulations can reproduce most winged and X-shaped sources with subsonic expansion if the AGN outburst is between 10–100 Myr old instead of 1–10 Myr. These simulations are also not the final word, as they only solve the equations of hydrodynamics in a relaxed, non-dynamic atmosphere.

5.2. Assessment

Our results, taken in context, strongly implicate a hydrodynamic origin for X-shaped sources and a common origin for winged and X-shaped sources. We can produce bona fide XRGs (i.e. with intrinsic $W/L > 0.8$) with a single outburst from a jet with a plausible time dependent kinetic luminosity on timescales broadly consistent

with observed sources. The radio galaxies we produce are consistent with prior simulations, and faithful reproductions of observed radio galaxies can be generated by tuning the viewing angle (Figure 11). These sources are also consistent with most observed properties of the XRG population outlined above, and our simulations reproduce elements of the overpressured cocoon and buoyant backflow models while relying solely on the interaction of the radio lobe material with an anisotropic environment. Hence, the backflow model remains a strong contender for the origin of XRGs—it would be surprising if some XRGs were *not* produced in this manner.

However, our simulations also present new challenges to the proposals in the literature: we find that long wings require unusually elliptical atmospheres and expand subsonically, making very long wings difficult to explain. Having examined the deficiencies of our simulations, we cannot identify an obvious internal remedy; we note that pre-existing channels are necessary (in the backflow model) for some sources in the literature and may be generally important.

The final prediction of our simulations is therefore that the XRG population is heterogeneous and *the backflow model works in tandem with other hydrodynamic models rather than solely on its own*. In short, this is because our models make it too difficult to produce XRGs given

their observed frequency.

Consider that winged and X-shaped sources make up 5–10% of double-lobed radio sources. If, as in our models, X-shaped sources are produced by a fortunate coincidence of jet geometry, ISM ellipticity, and jet power, we might imagine that the fraction of X-shaped sources is some function of each of these variables. In the simplest case, where each of these factors contribute independently to promoting wings, the fraction of XRGs might look like

$$f_{\text{XRG}} \propto f_{\text{PA}}^{\alpha} f_{\epsilon}^{\beta} f_{\text{kin},L}^{\gamma}, \quad (14)$$

where f_{XRG} is the fraction of double-lobed sources which are X-shaped and the other f values represent the fraction of sources for each variable which meet the threshold criterion for wings. The exponents are unknown measures of the relative importance of each variable. Obviously, the fraction of XRGs must be smaller than the fraction of sources which meet any one criterion.

Now, consider that virtually all double-lobed radio galaxies emanate from elliptical hosts, and have apparently random jet–major axis orientations (as opposed to the very weakest radio-emitting AGN whose jets seem to be pointed along the minor axis of their hosts; Browne & Battye 2010). Our models suggest that a jet within $\sim 15^\circ$ of the major axis of its host is required to produce wings. In a uniform distribution of radio jet position angles, we would thus expect that $f_{\text{PA}} \sim 15/90 \approx 0.17$. Assuming all powerful jets have a kinetic luminosity function conducive to forming XRGs, we still require about half of all sources where the jet is co-aligned with the major axis to have high ellipticity (assuming the exponents are all equal to unity). Given that ellipticity is clearly a very sensitive parameter and that the peak ϵ of powerful radio galaxy hosts is far below the wing threshold (Smith & Heckman 1989), it is clear that our simulations (in this oversimplified formulation) underpredict the observed frequency of winged sources. In other words, wings are *too difficult* to make in our models.

To reconcile this result with the observations, either our models must be fundamentally deficient with respect to the behavior of backflow or they require alternate mechanisms to form proto-wing channels such as the jet–stellar shell interaction model of Gopal-Krishna & Wiita (2010) or the jet–merging ISM explanation for Z-shaped sources in Zier (2005). As we have seen, backflowing material reinforces any proto-wings and can turn them into full-fledged wings if the original mechanism fails to do so; making the channels in the first place is what the backflow model cannot easily do.

Thus, we propose that the backflow model has a commensal relationship with other hydrodynamic mechanisms for forming wings by reinforcing and growing any pre-existing channels accessible to a jet pointed along the major axis of its host galaxy. These channels would naturally grow most easily along the steepest pressure gradient. In cases where the jet power and atmosphere size match appropriately, these channels would be produced by the expansion of an overpressured cocoon as in our simulations. In other cases, channels could be produced by the interaction of the jet with structure in the ISM or by minor mergers. In this scenario, we would still expect to see most of the predictions of our simulations

listed above for the case of pure backflow in a relaxed atmosphere.

5.3. Distortions to the Canonical Double-Lobed FR II Radio Galaxy

At this point, it is worth revisiting the buoyant backflow model as phrased in Leahy & Williams (1984), where XRGs are unified with other distortions to the canonical FR II model (about two thirds of strongly bridged radio galaxies show central distortions) by the deflection of backflow around a denser medium. These distortions may also be related to radio galaxies with interrupted bridges by the “superdisk” model (Gopal-Krishna & Wiita 2009), in which gas displaced by a galaxy merger is believed responsible for docking the lobes in an asymmetric manner.

Because the backflow model as expressed in our simulations depends only on a fortuitous combination of atmosphere morphology and jet behavior to produce winged sources, we can indeed reproduce the basic bridge distortions of Leahy & Williams (1984). However, we cannot reproduce long Z-shaped sources and some asymmetric distortions which do not appear to be the result of bulk motion or cluster turbulence. These include sources with a single wing on one side, sources with wings which themselves bend dramatically, sources with one FR I lobe and one FR II lobe (HYMORs; Gopal-Krishna & Wiita 2000). Again, the main hindrance seems to be the inability to channel backflow; jets which bend may solve this problem. Although there are elements of the behavior of backflow which we do not presently understand, we come to the same conclusion as with X-shaped sources: the backflow model can account for other bridged distortions only in tandem with another hydrodynamic mechanism.

6. SUMMARY AND CONCLUSIONS

We have conducted a series of three-dimensional hydrodynamic simulations of light, hypersonic jets to study the viability of the backflow model for the formation of wings in X-shaped radio galaxies. The XRGs seem to be a population unto themselves, with characteristic environmental geometry, radio power, black hole mass, etc., and any successful model must account for these peculiarities. Our main results follow.

1. The jets, back-flows, and lobes in our simulations are similar to those in the recent literature, giving us confidence in the usefulness of our simulations as probes of the backflow model.
2. Wings in our models form in two stages: the establishment of channels or proto-wings and then buoyant (usually subsonic) expansion. Specifically, our models corroborate the overpressured cocoon model of Capetti et al. (2002) early on, but as cocoons quickly come to pressure equilibrium with their surroundings, most of the wing length represents subsonic expansion (Figure 3).
3. We have produced prominent wings by geometry and radio power alone, proving that the backflow model can, in principle, make X-shaped sources (Figure 2.2 and 11). Both the atmosphere and jet

kinetic luminosity as a function of time are crucial to forming X-shaped sources.

4. Long wings are produced in a relatively small portion of parameter space, requiring galaxies with high ellipticity, decaying jets, proper jet orientation, and appropriate atmosphere size (Figures 7 and 8).
5. The main challenges to the backflow model are the requirement for high ellipticity and subsonic wing growth. Adding additional physics is not obviously helpful. The backflow model seems to require an additional mechanism to make proto-wings which the backflow reinforces; in our models, we make these channels by the initial expansion of an over-pressured cocoon in an anisotropic environment, but this cannot explain every XRG. We cannot form new channels solely by deflecting back-flows.
6. If the backflow model can overcome the issues noted above, it is a very strong candidate for explaining X-shaped and other disturbed radio galaxies. Our models naturally reproduce many of the characteristics of the XRG population (Table 4).

There are several natural extensions of this work which promise to be fruitful. First, adding magnetic fields and investigating other potential collimating mechanisms may rule out or boost the backflow model depending on the wing expansion speeds attained. Second, our models rely on the formation of channels misaligned with the jets; these have been proposed in several other contexts as well to explain radio galaxy morphology. The origin of these channels is not known, and identifying and testing candidates would be important for wing formation models. Third, more realistic jets could determine whether the backflow model can support both long wings and active FR II lobes with hot spots; the bending of the jets in particular is an important issue. Finally, models which produce the wings hydrodynamically but not explicitly by the deflection of backflow (e.g. the recently proposed stellar shell model Gopal-Krishna & Wiita 2010) are worth exploring by making the atmospheres more complex in tandem with more realistic jets.

The authors thank the anonymous referee for helpful and clarifying comments. We acknowledge support from *Chandra* grant GO011138A.

REFERENCES

- Alexander, P., & Leahy, J. P. 1987, *MNRAS*, 225, 1
 Antonuccio-Delogu, V., & Silk, J. 2010, *MNRAS*, 405, 1303
 Begelman, M. C. 2001, in *Astronomical Society of the Pacific Conference Series*, Vol. 240, *Gas and Galaxy Evolution*, ed. J. E. Hibbard, M. Rupen, & J. H. van Gorkom, 363–+
 Belan, M., de Ponte, S., Tordella, D., Massaglia, S., Ferrari, A., Mignone, A., & Bodenschatz, E. 2011, *ArXiv e-prints*
 Best, P. N. 2009, *Astronomische Nachrichten*, 330, 184
 Blanton, E. L., Randall, S. W., Douglass, E. M., Sarazin, C. L., Clarke, T. E., & McNamara, B. R. 2009, *ApJ*, 697, L95
 Bodo, G., Rossi, P., Massaglia, S., Ferrari, A., Malagoli, A., & Rosner, R. 1998, *A&A*, 333, 1117
 Braithwaite, J. 2010, *MNRAS*, 807
 Browne, I. W. A., & Battye, R. A. 2010, *ArXiv e-prints*
 Capetti, A., Zamfir, S., Rossi, P., Bodo, G., Zanni, C., & Massaglia, S. 2002, *A&A*, 394, 39
 Carvalho, J. C., & O’Dea, C. P. 2002a, *ApJS*, 141, 337
 —. 2002b, *ApJS*, 141, 371
 Cavaliere, A., & Fusco-Femiano, R. 1976, *A&A*, 49, 137
 Cheung, C. C. 2007, *AJ*, 133, 2097
 Cheung, C. C., Healey, S. E., Landt, H., Verdoes Kleijn, G., & Jordán, A. 2009, *ApJS*, 181, 548
 Churazov, E., Brüggen, M., Kaiser, C. R., Böhringer, H., & Forman, W. 2001, *ApJ*, 554, 261
 De Young, D. S. 2010, *ApJ*, 710, 743
 Dennett-Thorpe, J., Scheuer, P. A. G., Laing, R. A., Bridle, A. H., Pooley, G. G., & Reich, W. 2002, *MNRAS*, 330, 609
 Diehl, S., & Statler, T. S. 2007, *ApJ*, 668, 150
 Dong, R., & Stone, J. M. 2009, *ApJ*, 704, 1309
 Ekers, R. D., Fanti, R., Lari, C., & Parma, P. 1978, *Nature*, 276, 588
 Evans, D. A., et al. 2008, *ApJ*, 675, 1057
 Fabian, A. C., Sanders, J. S., Taylor, G. B., Allen, S. W., Crawford, C. S., Johnstone, R. M., & Iwasawa, K. 2006, *MNRAS*, 366, 417
 Falceta-Gonçalves, D., Caproni, A., Abraham, Z., Teixeira, D. M., & de Gouveia Dal Pino, E. M. 2010, *ApJ*, 713, L74
 Fanaroff, B. L., & Riley, J. M. 1974, *MNRAS*, 167, 31P
 Gabuzda, D. C., Murray, É., & Cronin, P. 2004, *MNRAS*, 351, L89
 Gaibler, V., Khochfar, S., & Krause, M. 2010, *ArXiv e-prints*
 Gopal-Krishna, Biermann, P. L., Gergely, L. Á., & Wiita, P. J. 2010, *ArXiv e-prints*
 Gopal-Krishna, Biermann, P. L., & Wiita, P. J. 2003, *ApJ*, 594, L103
 Gopal-Krishna, & Wiita, P. J. 2000, *A&A*, 363, 507
 —. 2009, *New A*, 14, 51
 —. 2010, *New A*, 15, 96
 Hayes, J. C., Norman, M. L., Fiedler, R. A., Bordner, J. O., Li, P. S., Clark, S. E., ud-Doula, A., & Mac Low, M. 2006, *ApJS*, 165, 188
 Heinz, S., Brüggen, M., Young, A., & Levesque, E. 2006, *MNRAS*, 373, L65
 Hodges-Kluck, E. J., Reynolds, C. S., Cheung, C. C., & Miller, M. C. 2010, *ApJ*, 710, 1205
 Huarte-Espinosa, M., Krause, M., & Alexander, P. 2010, *ArXiv e-prints*
 Kawakatu, N., Kino, M., & Nagai, H. 2009, *ApJ*, 697, L173
 Keppens, R., Meliani, Z., van der Holst, B., & Casse, F. 2008, *A&A*, 486, 663
 Komissarov, S. S., & Falle, S. A. E. G. 1996, in *Astronomical Society of the Pacific Conference Series*, Vol. 100, *Energy Transport in Radio Galaxies and Quasars*, ed. P. E. Hardee, A. H. Bridle, & J. A. Zensus, 173–+
 Kraft, R. P., Hardcastle, M. J., Worrall, D. M., & Murray, S. S. 2005, *ApJ*, 622, 149
 Krause, M. 2003, *A&A*, 398, 113
 —. 2005, *A&A*, 431, 45
 Lal, D. V., & Rao, A. P. 2005, *MNRAS*, 356, 232
 —. 2007, *MNRAS*, 374, 1085
 Landt, H., Cheung, C. C., & Healey, S. E. 2010, *ArXiv e-prints*
 Leahy, J. P., & Parma, P. 1992, in *Extragalactic Radio Sources. From Beams to Jets*, ed. J. Roland, H. Sol, & G. Pelletier, 307–308
 Leahy, J. P., & Williams, A. G. 1984, *MNRAS*, 210, 929
 Ledlow, M. J., & Owen, F. N. 1996, *AJ*, 112, 9
 Ly, C., De Young, D. S., & Bechtold, J. 2005, *ApJ*, 618, 609
 Merritt, D., & Ekers, R. D. 2002, *Science*, 297, 1310
 Mezcuca, M., Lobanov, A. P., Chavushyan, V. H., & León-Tavares, J. 2010, *ArXiv e-prints*
 Mignone, A., Rossi, P., Bodo, G., Ferrari, A., & Massaglia, S. 2010, *MNRAS*, 402, 7
 Morsony, B. J., Heinz, S., Brüggen, M., & Ruszkowski, M. 2010, *ArXiv e-prints*
 Murgia, M., Parma, P., de Ruiter, H. R., Bondi, M., Ekers, R. D., Fanti, R., & Fomalont, E. B. 2001, *A&A*, 380, 102
 Omma, H., & Binney, J. 2004, *MNRAS*, 350, L13
 Omma, H., Binney, J., Bryan, G., & Slyz, A. 2004, *MNRAS*, 348, 1105

- O'Neill, S. M., De Young, D. S., & Jones, T. W. 2009, *ApJ*, 694, 1317
- O'Neill, S. M., & Jones, T. W. 2010, *ApJ*, 710, 180
- O'Neill, S. M., Tregillis, I. L., Jones, T. W., & Ryu, D. 2005, *ApJ*, 633, 717
- Ostriker, J. P., Choi, E., Ciotti, L., Novak, G. S., & Proga, D. 2010, *ArXiv e-prints*
- Perlman, E. S., & Wilson, A. S. 2005, *ApJ*, 627, 140
- Pope, E. C. D., Babul, A., Pavlovski, G., Bower, R. G., & Dotter, A. 2010, *MNRAS*, 851
- Reynolds, C. S., Heinz, S., & Begelman, M. C. 2002, *MNRAS*, 332, 271
- Rosario, D. J., Whittle, M., Nelson, C. H., & Wilson, A. S. 2010, *ApJ*, 711, L94
- Rosen, A., Hughes, P. A., Duncan, G. C., & Hardee, P. E. 1999, *ApJ*, 516, 729
- Rottmann, H. 2001, PhD Thesis
- Ruszkowski, M., Enßlin, T. A., Brüggén, M., Heinz, S., & Pfrommer, C. 2007, *MNRAS*, 378, 662
- Saripalli, L., & Subrahmanyam, R. 2009, *ApJ*, 695, 156
- Saxton, C. J., Wu, K., Korunoska, S., Lee, K., Lee, K., & Beddows, N. 2010, *MNRAS*, 594
- Simionescu, A., Roediger, E., Nulsen, P. E. J., Brüggén, M., Forman, W. R., Böhringer, H., Werner, N., & Finoguenov, A. 2009, *A&A*, 495, 721
- Smith, E. P., & Heckman, T. M. 1989, *ApJ*, 341, 658
- Stone, J. M., & Norman, M. L. 1992a, *ApJS*, 80, 753
- . 1992b, *ApJS*, 80, 791
- Sun, M., Voit, G. M., Donahue, M., Jones, C., Forman, W., & Vikhlinin, A. 2009, *ApJ*, 693, 1142
- Sutherland, R. S., & Bicknell, G. V. 2007, *ApJS*, 173, 37
- Vernaleo, J. C., & Reynolds, C. S. 2006, *ApJ*, 645, 83
- . 2007, *ApJ*, 671, 171
- Worrall, D. M., Birkinshaw, M., & Cameron, R. A. 1995, *ApJ*, 449, 93
- Zanni, C., Massaglia, S., Bodo, G., Rossi, P., Capetti, A., & Ferrari, A. 2003, *Memorie della Societa Astronomica Italiana Supplementi*, 1, 155
- Zier, C. 2005, *MNRAS*, 364, 583
- Zier, C., & Biermann, P. L. 2001, *A&A*, 377, 23